RESEARCH ARTICLE | FEBRUARY 06 2023

Initial stages of gravity-driven flow of two fluids of equal depth ⊘

Alexander Korobkin [iD] ; Oguz Yilmaz ✉ [iD]

Check for updates

View Online   Export Citation   CrossMark

Initial stages of gravity-driven flow of two fluids of equal depth

View Online   Export Citation   CrossMark

Alexander Korobkin[1] (iD) and Oguz Yilmaz[2,a)] (iD)

AFFILIATIONS

[1]School of Mathematics, University of East Anglia, Norwich, United Kingdom
[2]Department of Mathematics, Izmir Institute of Technology, Urla 35430, Izmir, Türkiye

[a)]Author to whom correspondence should be addressed: oguzyilmaz@iyte.edu.tr

ABSTRACT

Short-time behavior of gravity-driven free surface flow of two fluids of equal depth and different densities is studied. Initially, the fluids are at rest and separated with a vertical rigid plate of negligible thickness. Then, the plate disappears suddenly and a gravity-driven flow of the fluids starts. The flow in an early stage is described by the potential theory. The initial flow in the leading order is described by a linear problem, which is solved by the Fourier series method. The motions of the interface between the fluids and their free surfaces are investigated. The singular behaviors of the velocity field at the bottom point, where the interface meets the rigid bottom, and the top point, where the interface meets both free surfaces, are analyzed in detail. The flow velocity is shown to be log-singular at the bottom point. The leading-order inner asymptotic solution is constructed in a small vicinity of this point. It is shown that the flow close to the bottom point is self-similar. The motion of the interface is independent of any parameters, including the density ratio, of the problem in specially stretched variables. In the limiting case of negligible density of one of the fluids, the results of the classical dam break problem are recovered. The Lagrangian representation is employed to capture the behavior of the interface and the free surfaces at the top, where the fluid interface meets the free surfaces. The shapes of the free surfaces and the interface in the leading order computed by using the Lagrangian variables show a jump discontinuity of the free surface near the top point where the free surfaces and the interface meet. Inner region formulation is derived near the top point.

Published under an exclusive license by AIP Publishing. https://doi.org/10.1063/5.0138868

I. INTRODUCTION

The two-dimensional irrotational flow generated by the removal of a vertical plate, which separates two fluids of equal height and different densities, is investigated for short times. The resulting motion is known as gravity currents in the literature. Gravity currents occur when a denser fluid surges under a lighter fluid. The resulting flow is controlled by the interaction between the fluids. If the presence of the lighter fluid can be neglected, the flow is known as a dam break flow.

Gravity currents play an important role in many natural situations and also in engineering applications. Examples of gravity currents are sea breeze fronts in the atmosphere,[1] atmospheric pollution, base surges produced by volcanic eruptions, and ocean currents driven by salinity and temperature differences.[2] Industrial problems with gravity-driven flows include entomology and pest control, aircraft safety, and dense gas technology where gravity currents of a dense gas and oil spillage on the sea surface[3] may be formed in an industrial accident. Simpson gave an excellent review of gravity currents.[4] A gravity current can be set up in experiments by removing a vertical

lock gate, which separates two fluids. The resulting flow is also known as the lock exchange flow. An experimental investigation of the long time behavior of flows where a finite volume of a fluid has been released into another surrounding fluid of slightly lower density was carried out by Rottman *et al.*[5] Experiments were performed in a channel of rectangular cross section. Qualitatively, accurate results were obtained for $0 < h_0/H \leq 1$, where h_0 is the initial depth of the released heavier fluid and H is the depth of the ambient lighter fluid in the channel. Numerical and asymptotic analyses of gravity currents for large times using shallow water equations were done by D'alessio *et al.*[6] They concluded that there is a critical value for the initial fractional depth occupied by the heavier fluid h_0/H above which a second bore is formed behind the leading one and eventually overtakes it. There are also numerical investigations, which consider two-layer gravity currents in a two-dimensional rectangular channel.[7,8] All investigations mentioned above are concerned with the large-time behavior of the gravity current flows as opposed to the short-time behavior studied in this paper. The singularities examined in the

present study are important for improving accuracy and efficiency of the numerical calculations. Also, the jet formations and the vortices occurring at these special locations are interesting from both physical and mathematical points of view.

The short-time asymptotic solutions can explain the structure of the initial flow, which could be singular and difficult to be described by pure numerical means which work well for smooth, "well-behaved" flows. The failure of numerical methods for short times near "contact points" where boundary and initial conditions do not match each other and where singularities are likely to occur was also mentioned by Tyvand and Miloh.[9] In that paper, the authors analytically studied the impulsively starting motion of a circular cylinder submerged below a free surface using a short-time expansion. It was claimed that numerical solutions of the fully nonlinear initial boundary-value problem for an impulsively started submerged cylinder cannot give accurate predictions of the hydrodynamic forces for short times. Our arguments in this paper are similar to those by Tyvand and Miloh:[9] initial transient flows near some special points are described in a more reliable way by asymptotic analysis rather than by pure numerical calculations.

Existing studies of two-fluid gravity currents consider flows in channels with rigid covers. There are very few papers on two-fluid gravity currents with free surfaces. Adduce *et al.*[10] investigated free surface effects using experimental measurements and a mathematical model based on shallow water equations. The front position and speed of the current were predicted for large times taking into account the entrainment at the interface as well as the free surface effects. It was claimed in Ref. [10] that there are "three different stages in the gravity current dynamics: a first slumping phase, in which the front speed is time-constant; a second self-similar phase with a decelerating front velocity; and a third viscous phase, when viscous effects are prevalent."

In the present paper, we investigate the short-time behavior of gravity-driven free surface flows of two fluids of equal depth and different densities. This problem, to the best of our knowledge, has not been studied before. Initial asymptotics of inertia dominated flows were studied in Refs. [11–15]. This is a gravity current problem with account for free-surface effects studied for short times. Viscous effects on the current are negligible for short times, which is justified at the end of Sec. VI. The uniformly valid asymptotic solution of this problem is obtained using the method of matched asymptotic expansions. First, the leading-order solution in the main flow region is determined by the Fourier method. This solution is singular at the two contact points between the fluid interface and other boundaries of the fluids. We investigate details of the local flow close to the singular point at the bottom, where the two fluids meet and a jet formation is expected similar to that in the classical dam break problem.[16] The flow velocity predicted by the leading-order solution at the top point, where the free surfaces of the two fluids meet the interface, is shown to be unbounded and inversely proportional to the distance to this point. The problem involving fluids of different depths was studied by the authors of this paper in Ref. [17] where the leading-order solution also predicted unbounded flow velocity at the corner point, where the interface between the two fluids meets the free surfaces of the fluids, but the singularity of the velocity field was weaker than the one in the present problem.

The present analysis is a natural extension of the classical dam break problem, where a fluid is only on one side of the wall,[16] and the

wet bed dam break problem where two fluids of different depths are on either side of the wall.[17] In the wet bed problem, there are two singular points at the interface with a logarithmic singularity at the bottom point and a power singularity at the top of the interface, where the fluid interface meets the free surfaces of the fluids. Jetting on a liquid-free surface was studied in Ref. [18]. In the present paper, as a special case of the wet bed problem, we consider the fluids of equal depth and different densities separated initially by a vertical wall. We observe that, in this special case, while the power singularity at the top of the interface is modified, the logarithmic singularity at the bottom of the interface persists. Correspondingly, the local flow close to the bottom contact point is similar, but not identical, to the flow studied in Ref. [16] for the classical dam break problem. The latter flow is similar to the local flow studied in Ref. [19] for a problem of a vertical wall impact onto a liquid layer. The inner solution constructed in the present paper near the bottom contact point is valid also for fluids of different depths,[17] with some modifications of the matching conditions.

The problem is formulated in Sec. II assuming immiscible, inviscid, and incompressible fluids. The leading-order and the second-order solutions are derived in Secs. III and IV, respectively. In Secs. III and IV, we employ the Lagrangian representation to correctly capture the behavior of the interface and the free surfaces at the top where the interface meets the free surfaces. The leading-order solution is singular at the bottom point where we derive an inner solution, see Sec. V. The obtained solution is compared to that of the classical dam break problem to investigate the effect of the second fluid on the gravity-driven unsteady flow along the bottom. Another singular point of the flow is where the interface of the fluids meets their free surfaces. The leading-order outer solution predicts unbounded velocity field there. The problem, which describes the local flow there in stretched coordinates, is derived in Sec. VI. Finally, it is justified that the viscous effects can be neglected at the leading order both in the main flow region and for the local flows near these special points. Some conclusions are drawn in Sec. VII.

II. FORMULATION OF THE PROBLEM

Initially, two fluids of the same depth H and different densities, ρ^- in $x' < 0$ and ρ^+ in $x' > 0$, are kept apart by a vertical wall of zero thickness at $x' = 0$. Primes stand for dimensional variables. The fluids are bounded by the free surfaces, $y = H, x' < 0$, and $y = H, x' > 0$ from above and by the rigid bottom, $y' = 0$, from below, see Fig. 1(a). The fluids are at rest. At $t' = 0$, the wall is suddenly removed and the gravity-driven flow of the fluids starts. The interface between the two fluids is created instantly at $t' = 0$. At the interface, the normal velocities and the hydrodynamic pressures of the fluids are equal at any time of the flow, $t' > 0$. The hydrostatic pressures on the left and the right-hand sides of the wall are different at $t' = 0$. The instantaneous adjustment of the pressure at the interface $x' = 0$ immediately after the removal of the wall forces the two fluids to flow. The sketch of the resulting flow is shown in Fig. 1(b).

We shall determine the unsteady two-dimensional flow and the motions of the fluid boundaries during the initial stage, when the fluid displacements are small compared with their initial depth H. Particular attention will be given to the local flows close to the points, where the interface meets the bottom and the free surfaces of the fluids.
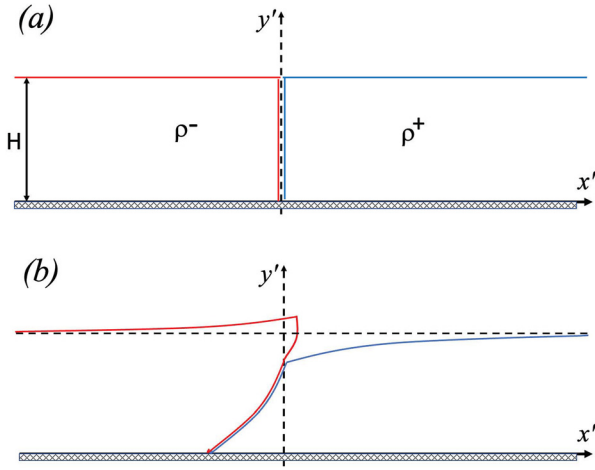
FIG. 1. (a) Two immiscible, inviscid, and incompressible fluids with densities ρ^+ and ρ^- are separated initially by the thin vertical wall at $x' = 0$. (b) Sketch of the dam-break flow of two immiscible fluids.

The fluids are assumed immiscible, inviscid, and incompressible. Without loss of generality, let $\rho^+ \geq \rho^-$. If the density ratio $\gamma = \rho^-/\rho^+$ is equal to one, there is no flow induced by the removal of the wall. If $\gamma \to 0$, we arrive at the classical dam break flow without the lighter fluid. The flow for $0 < \gamma < 1$ is assumed two-dimensional and irrotational. Quantities describing the fluid on the right of the wall are denoted by the superscript $+$ and on the left of the wall by $-$. Surface tension and the presence of air are not taken into account. The initial hydrostatic pressures are

$$
\begin{aligned}
p'^+(x', y', 0^-) &= \rho^+ g(H - y'), \quad x' > 0, \\
p'^-(x', y', 0^-) &= \rho^- g(H - y'), \quad x' < 0,
\end{aligned} \tag{1}
$$

where g is the gravitational acceleration and the atmospheric pressure is taken as the reference one.

The gravity-driven flow is described by the velocity potentials $\varphi^\pm(x, y, t)$ in the dimensionless variables

$$
\begin{aligned}
x' &= Hx, \quad y' = Hy, \quad t' = Tt, \quad \varphi'^\pm = gHT\varphi^\pm, \\
p'^\pm &= \rho^\pm gHp^\pm, \quad T = \epsilon^{\frac{1}{2}}\sqrt{H/g}, \quad \gamma = \rho^-/\rho^+,
\end{aligned} \tag{2}
$$

where a small positive parameter ϵ is introduced to indicate that the early stage of the flow is of primary interest in this study. Shapes of the free surfaces are described by the equations

$$
y' = H + Y'^\pm(x', t'), \tag{3a}
$$

or in the dimensionless variables,

$$
y = 1 + \epsilon Y^\pm(x, t), \tag{3b}
$$

where the vertical displacements of the free surfaces are scaled as

$$
Y'^\pm = \epsilon H Y^\pm(x, t). \tag{4a}
$$

The shape of the interface is described by the equation

$$
x = \epsilon X(y, t), \tag{4b}
$$

where $X' = \epsilon H X(y, t)$ and $x' = X'(y', t')$ in the dimensional variables. The functions $H^\pm(x, t)$ in (4a) and $X(y, t)$ in (4b), including their

spatial domains, are unknown in advance and should be determined as part of the solution.

The flow regions $\Omega^\pm(t)$ are time-dependent. The boundary value problem for the velocity potentials $\varphi^\pm(x, y, t)$, the free surface elevations $Y^\pm(x, t)$, and the displacement of the interface $X(y, t)$ reads

$$
\Delta\varphi^\pm = 0 \quad (\text{in } \Omega^\pm), \tag{5}
$$

$$
\varphi_t^\pm = -\epsilon\left(\frac{1}{2}|\nabla\varphi^\pm|^2 + Y^\pm\right) \quad (\text{on } y = 1 + \epsilon Y^\pm(x, t)), \tag{6}
$$

$$
Y_t^\pm = \varphi_y^\pm - \epsilon Y_x^\pm \varphi_x^\pm \quad (\text{on } y = 1 + \epsilon Y^\pm(x, t)), \tag{7}
$$

$$
\begin{aligned}
\varphi_t^+ &- \gamma\varphi_t^- + y(1 - \gamma) + \gamma - 1 \\
&= \frac{1}{2}\epsilon(\gamma|\nabla\varphi^-|^2 - |\nabla\varphi^+|^2) \quad (\text{on } x = \epsilon X(y, t)),
\end{aligned} \tag{8}
$$

$$
X_t = \varphi_x^\pm - \epsilon X_y \varphi_y^\pm \quad (\text{on } x = \epsilon X(y, t)), \tag{9}
$$

$$
\varphi_y^\pm = 0 \quad (y = 0), \tag{10}
$$

$$
\varphi^\pm \to 0 \quad (x \to \pm\infty), \tag{11}
$$

$$
\varphi^\pm = 0, \quad Y^\pm = 0, \quad X = 0 \quad (t = 0). \tag{12}
$$

The potentials $\varphi^\pm(x, y, t)$ satisfy the Laplace equations (5) in their respective regions, $\Omega^\pm(t)$, the dynamic and kinematic boundary conditions, (6) and (7), on the free surfaces $y = 1 + \epsilon Y^\pm(x, t)$, the dynamic and kinematic interface conditions, (8) and (9), the slip boundary condition at the bottom (10), conditions at infinity (11), and the initial conditions (12). The triple point, at which the interface and the free surfaces meet, is not a material point, in general. The fluids can slide with respect to each other at the interface. The triple point, where the interface meets the bottom, is a material point in this study. Both triple points require local analyses of the flows near these points. These points are singular points of the asymptotic solutions in the main flow regions as $\epsilon \to 0$.

III. THE LEADING-ORDER OUTER SOLUTION

The solution of the problem (5)–(12) for small ϵ is sought in the form

$$
\varphi^\pm(x, y, t, \epsilon) = t\varphi_0^\pm(x, y) + \frac{1}{6}\epsilon t^3 \varphi_1^\pm(x, y) + \cdots,
$$

$$
Y^\pm(x, t, \epsilon) = \frac{1}{2}t^2 \varphi_{0,y}^\pm(x, 1) + \frac{1}{24}\epsilon t^4 Y_1^\pm(x) + \cdots, \tag{13}
$$

$$
X(y, t, \epsilon) = \frac{1}{2}t^2 \varphi_{0,x}^\pm(0, y) + \frac{1}{24}\epsilon t^4 X_1(y) + \cdots.
$$

By substituting expansions (13) in Eqs. (5)–(12) and setting $\epsilon = 0$, we arrive at the boundary value problem for the leading-order velocity potentials

$$
\begin{aligned}
\Delta\varphi_0^+ &= 0 \ (x > 0, 0 < y < 1), \quad \Delta\varphi_0^- = 0 \ (x < 0, 0 < y < 1), \\
\varphi_0^\pm &= 0 \ (y = 1), \quad \varphi_{0,y}^\pm = 0 \ (y = 0), \\
\varphi_0^+ &- \gamma\varphi_0^- + y(1 - \gamma) + \gamma - 1 = 0, \\
\varphi_{0,x}^+ &= \varphi_{0,x}^- \ (x = 0, 0 < y < 1), \quad \varphi_0^\pm \to 0 \ (x \to \pm\infty).
\end{aligned} \tag{14}
$$

While the boundary conditions at the upper triple point $(0, 1)$ match each other, those at the lower triple point $(0, 0)$ do not. The horizontal velocities $\varphi_{0,x}^\pm$ are continuous at the interface, but the velocity potentials are not.

The velocity potentials $\varphi_0^{\pm}(x, y)$ are sought in the form

$$\varphi_0^+(x, y) = \sum_{n=0}^{\infty} c_n e^{-\mu_n x} \cos(\mu_n y),$$

$$\varphi_0^-(x, y) = \sum_{n=0}^{\infty} d_n e^{\mu_n x} \cos(\mu_n y),$$

(15)

where $\mu_n = \frac{\pi}{2}(2n+1)$, $x > 0$ for $\varphi_0^+(x, y)$ and $x < 0$ for $\varphi_0^-(x, y)$. The potentials (15) satisfy all equations in (14) except for the conditions at the interface, $x = 0$. The condition $\varphi_{0,x}^+ = \varphi_{0,x}^-$ at $x = 0$ gives $-c_n = d_n$, and the dynamic condition at the interface gives

$$\frac{1}{2}(c_n - \gamma d_n) = \frac{1}{\mu_n^2}(1 - \gamma).$$

Combining both equations, we obtain

$$c_n = \frac{2\delta}{\mu_n^2}, \quad d_n = -c_n,$$

(16)

where $\delta = (1 - \gamma)/(1 + \gamma)$. Therefore,

$$\varphi_0^-(x, y) = -\varphi_0^+(-x, y) \quad (x < 0),$$

(17)

$$\varphi_0^+(x, y) = \delta\varphi_{00}(x, y),$$

$$\varphi_{00}(x, y) = 2\sum_{n=0}^{\infty} \frac{1}{\mu_n^2} e^{-\mu_n x} \cos(\mu_n y),$$

(18)

where $\varphi_{00}(x, y)$ is the potential of the classical dam break problem corresponding to $\gamma = 0$ (Ref. 16). The obtained solution implies that the deflection of the interface in the leading order is equal to the deflection of the initially vertical free surface of the dam break flow multiplied by δ. Since $\delta < 1$, the presence of the lighter fluid reduces the displacement of the heavier fluid. The displacement of the interface is zero for $\delta = 0$, which is for fluids of equal densities.

Equations (13), (17), and (18) provide

$$Y^{\pm}(0, t) = \mp \frac{\delta}{2} t^2,$$

at the leading order as $\epsilon \to 0$. This suggests that the free surface of the heavier fluid on the right moves down and the left free surface of the lighter fluid moves upward. The lighter fluid is lifted to the height δt^2 relative to the heavier fluid on the right. We conclude that the leading-order solution (17) and (18) is not valid at the bottom intersection point (0, 0), where the horizontal velocity is log-singular[16] and at the triple point (0, 1), where discontinuous free surface is predicted by the leading order solution.

The positions of the free surfaces and the interface near the upper triple point are analyzed using the Lagrangian variables ξ, η of the fluid particles. The Eulerian coordinates x and y are considered as functions of ξ, η, and t, where $x = x(\xi, \eta, t)$, $y = y(\xi, \eta, t)$ and $x(\xi, \eta, 0) = \xi$, $y(\xi, \eta, 0) = \eta$. Displacements of the liquid particles, $x(\xi, \eta, t) - \xi$ and $y(\xi, \eta, t) - \eta$, are of order $O(\epsilon t^2)$ as $\epsilon \to 0$, see (13). The liquid particles of the free surfaces, $\xi > 0, \eta = 1$ and $\xi < 0$, $\eta = 1$ move only vertically in the leading order. Therefore, the Eulerian coordinates x and y in (17) and (18) can be approximated in the leading order by the Lagrangian coordinates ξ and η. Then, the positions of the free surfaces are given in the leading order by

$$y = 1 + \frac{\epsilon\delta}{2} t^2 \varphi_{00,y}(x, 1) \quad (x > 0),$$

$$y = 1 - \frac{\epsilon\delta}{2} t^2 \varphi_{00,y}(-x, 1) \quad (x < 0),$$

(19)

$$\varphi_{00,y}(x, 1) = -\frac{4}{\pi} \arctan(e^{-\pi x/2}) \quad (x > 0).$$

The free-surface elevations are asymmetric, proportional to δ and decay exponentially with the distance from the interface. The vertical and horizontal velocities at the interface, $\xi = 0, 0 < \eta < 1$, are of the same order as $\epsilon \to 0$,

$$\varphi_x^{\pm}(0, y, t, \epsilon) = \frac{2}{\pi} \delta t \log\left(\tan\left(\frac{\pi}{4} y\right)\right) + O(\epsilon t^3),$$

$$\varphi_y^{\pm}(0, y, t, \epsilon) = \mp \delta t + O(\epsilon t^3).$$

(20)

However, the shape of the interface is governed by the horizontal motion of the liquid particles at both sides of the interface. This is because the interface is still about vertical during the initial stage. The vertical displacements of the liquid particles along the interface do not change the shape of the interface significantly, except for the upper end of the interface, where the horizontal velocities are much smaller than the vertical velocities.

Figure 2 shows the shapes of free surfaces and interface in non-dimensional variables at leading order calculated using the Lagrangian variables. Approaching the triple point (0, 1), the lighter fluid on the left moves up and the heavier fluid on the right moves down. The shapes of the free surfaces and interface are close to straight lines near the triple point. The slopes of the free surfaces are 1/15, and the slope of the interface is 10.7 approximately. The leading-order solution predicts discontinuity at the triple point, which is not physical. For that reason, the shapes of the free surfaces and the interface close to the triple point are shown by dotted lines in the figure. Second-order solution and inner region solution near the triple point are required to resolve the discontinuity problem there. In drawing the figure, it was assumed that the interface is not
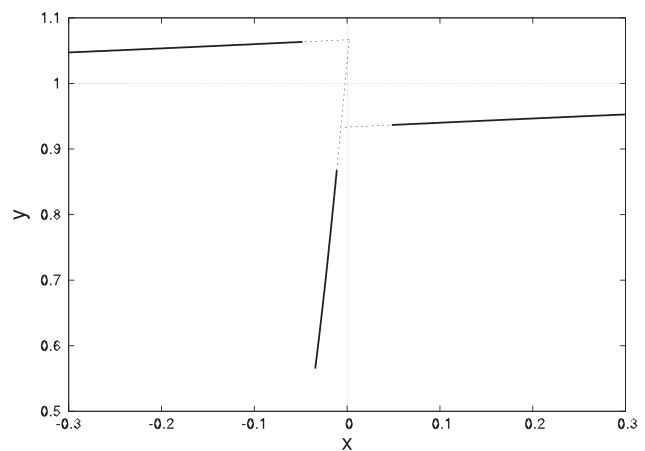
FIG. 2. The shapes of the free surfaces and the interface in the dimensionless variables at leading order computed by using the Lagrangian variables for $\gamma = 0.5$, $t = 1$, and $\epsilon = 0.4$.

a single material line so that the fluids can slide with respect to each other along the interface.

IV. SECOND-ORDER OUTER SOLUTION

The second-order outer solution is needed to increase the time interval of validity of the short-time solution (13), to obtain more details about the initial flow, to determine the size of the inner regions near the triple points, and to derive the matching conditions for the inner solutions. It will be shown in this section that the second-order solution approaches the corresponding solution of the classical dam break problem when the lighter fluid disappears, $\gamma \to 0$ and $\delta \to 1$. The presence of the lighter fluid makes the flow complicated with a point vortex at the upper triple point. The second-order flow velocities are singular also at the bottom triple point, $x = 0, y = 0$, similar to the flow near the bottom in the dam break problem for a single fluid, see Ref. 16. The second-order solution, as well as the solution of the original problem, decays as the densities of the fluids approach each other, $\gamma \to 1$ and correspondingly, $\delta \to 0$.

The second-order velocity potentials $\varphi_1^\pm(x, y)$ in the asymptotic expansions (13) satisfy Laplace's equation in the liquid regions, $x > 0, 0 < y < 1$ and $x < 0, 0 < y < 1$ and the bottom boundary condition (10). Both potentials decay at infinity, where $x \to \pm\infty$. The boundary conditions at the free surfaces and the interface are derived by using the asymptotic expansions of the boundary conditions (6)–(9) close to the initial positions of these boundaries and expansions (9). The dynamic and kinematic conditions on the free surfaces of the fluids, (6) and (7), give in the second order as $\epsilon \to 0$,

$$\varphi_1^\pm(x, 1) = -2(\varphi_{0,y}^\pm(x, 1))^2 - \varphi_{0,y}^\pm, \tag{21}$$

$$Y_1^\pm(x) = \varphi_{1,y}^\pm(x, 1), \tag{22}$$

where $x > 0$ for $\varphi_1^+(x, y)$ and $x < 0$ for $\varphi_1^-(x, y)$. The interface conditions (8) and (9) provide

$$\varphi_1^+ - \gamma \varphi_1^- = 2(\gamma - 1)(\varphi_{0,x}^+)^2 + \frac{(\gamma - 1)^3}{(\gamma + 1)^2}, \tag{23}$$

$$X_1(y) = \varphi_{1,x}^\pm(0, y) - 3\varphi_{0,y}^\pm(0, y)\varphi_{0,xy}^\pm(0, y) \ (x = 0, 0 < y < 1). \tag{24}$$

To simplify the boundary conditions (23) and (24) and to separate the singular part of the potentials at the bottom triple point, new potentials $\phi^\pm(x, y)$ are introduced by

$$\varphi_1^+ = \frac{2 + \gamma}{1 + \gamma} \left[(\varphi_{0,y}^+)^2 - (\varphi_{0,x}^+)^2 \right] + \phi^+, \tag{25}$$

$$\varphi_1^- = \frac{1 + 2\gamma}{1 + \gamma} \left[(\varphi_{0,y}^-)^2 - (\varphi_{0,x}^-)^2 \right] + \phi^-. \tag{26}$$

The potentials $\phi^\pm(x, y)$ satisfy Laplace's equations in the corresponding regions, the bottom condition, $\phi_y^\pm = 0$, where $y = 0$, and the following conditions on the free surfaces and the interface:

$$\phi^+ = -\varphi_{0,y}^+ - \frac{4 + 3\gamma}{1 + \gamma}(\varphi_{0,y}^+)^2 \ (y = 1, x > 0), \tag{27}$$

$$\phi^- = -\varphi_{0,y}^- - \frac{3 + 4\gamma}{1 + \gamma}(\varphi_{0,y}^-)^2 \ (y = 1, x < 0), \tag{28}$$

$$\phi^+ = \gamma\phi^- + 3\frac{(\gamma - 1)^3}{(\gamma + 1)^2}, \quad \phi_x^+ = \phi_x^- \ (x = 0, 0 < y < 1). \tag{29}$$

The boundary conditions (27)–(29) do not match each other at the triple point, $x = 0, y = 1$, where the interface meets the free surfaces of the fluids. Indeed, substituting $\varphi_{0,y}^\pm(0, 1) = \mp\delta$ in (27) and (28), we find

$$\phi^+(0, 1) = \frac{1 - \gamma}{(1 + \gamma)^3}(4\gamma^2 + 3\gamma - 3), \quad \phi^-(0, 1) = \frac{1 - \gamma}{(1 + \gamma)^3}(3\gamma^2 - 3\gamma - 4). \tag{30}$$

The values $\phi^+(0, 1)$ and $\phi^-(0, 1)$, where $0 \le \gamma < 1$, are not equal, and they do not satisfy the first condition in (29) on the interface. This implies that the potentials $\phi^\pm(x, y)$ are finite close to this triple point but are not continuous at this point. The local behavior of the potentials is described in the local polar coordinates (r, θ) by

$$\phi^\pm(r, \theta) \sim \frac{\Gamma}{2\pi}\theta + b^\pm \ (r \to 0), \tag{31}$$

where $x = r\cos\theta, y = 1 + r\sin\theta$; $\pi < \theta < \frac{3}{2}\pi$ for $\phi^-(r, \theta)$ and $\frac{3}{2}\pi < \theta < 2\pi$ for $\phi^+(r, \theta)$. The coefficients Γ and $b^\pm$ follow from (29) and (30):

$$\Gamma = 16\gamma\frac{1 - \gamma}{(1 + \gamma)^3}, \quad b^+ = \frac{1 - \gamma}{(1 + \gamma)^3}(4\gamma^2 - 13\gamma - 3),$$
$$b^- = \frac{1 - \gamma}{(1 + \gamma)^3}(3\gamma^2 - 11\gamma - 4). \tag{32}$$

The local asymptotic solution (31) predicts that the second-order vertical velocity on the free surface is singular

$$\phi_y^\pm(x, 1) \sim \frac{\Gamma}{2\pi x} \ (|x| \to 0). \tag{33}$$

Locally, the second-order velocity potentials are represented by a vortex centered at the triple point with the circulation Γ defined by (32). $\Gamma = 0$ when $\gamma = 0$ and $\gamma = 1$. The maximum $\Gamma = 5.18$ is achieved at $\gamma = 2 - \sqrt{3} \approx 0.268$. Therefore, for fluids with a density ratio of 0.268, the vortex at the upper triple point is the most intense.

The potentials $\phi^\pm(x, y)$ are decomposed into singular, $\phi_S^\pm(x, y)$, and regular, $\phi_R^\pm(x, y)$, components

$$\phi^\pm = \phi_S^\pm + \phi_R^\pm. \tag{34}$$

The singular potentials, $\phi_S^\pm(x, y)$, behave as (31) near the triple point $x = 0, y = 1$. These potentials are constructed by the method of images

$$\phi_S^\pm = Re\left[\left(\frac{\Gamma}{2\pi i}\log(z - i) + B^\pm \right) \frac{1}{(2 + iz)^2} \right.$$
$$\left. + \left(-\frac{\Gamma}{2\pi i}\log(z + i) + B^\pm \right) \frac{1}{(2 - iz)^2} \right], \tag{35}$$

where $B^\pm = \Gamma/40 + 9b^\pm/10$, $i = \sqrt{-1}$ and z is the complex variable, $z = x + iy$. The function $1/(2 + iz)^2$ is introduced to satisfy the condition at infinity, and the images are needed to satisfy the slip boundary condition at $y = 0$.

The potentials $\phi_R^\pm(x, y)$ are sought in the form

$$\phi_R^\pm(x, y) = \phi_{R0}(x, y) + \phi_{R1}^\pm(x, y), \tag{36}$$

where $\phi_{R0}(x, y)$ is continuous across the interface and satisfies together with the singular potentials (35), the free surface boundary
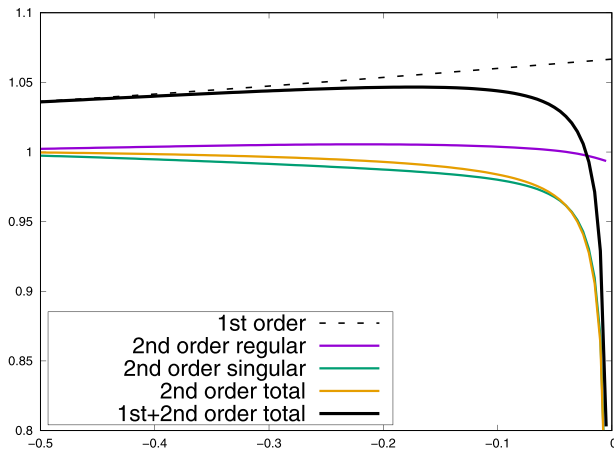
FIG. 3. The shape of the left free surface in the dimensionless variables for $\gamma = 0.5$, $t = 1$, and $\epsilon = 0.4$.

FIG. 5. The shape of the interface in the dimensionless variables for $\gamma = 0.5$, $t = 1$, and $\epsilon = 0.4$.

condition (27) and (28) on $y = 1$. The potential $\phi_{R0}(x, y)$ is obtained by the Fourier transform in x. The potentials $\phi_{R1}^{\pm}(x, y)$ are zero on the free surfaces, satisfy the bottom condition (10), and are sought in form (15). The details of the calculations of $\phi_{R0}(x, y)$ and $\phi_{R1}^{\pm}(x, y)$ are given in Appendix A.

Close to the triple point at the bottom, $x = 0$ and $y = 0$, the conditions (29) and the bottom condition, $\phi_y^{\pm}(x, 0) = 0$, match each other and the potentials $\phi^{\pm}(x, y)$ are regular at this point. However, the potentials $\varphi_1^{\pm}(x, y)$ given by (25) and (26) are singular there because $\varphi_{0,x}^{\pm}$ in (25) and (26) are log-singular at that point.

We conclude that the second-order potentials $\varphi_1^{\pm}(x, y)$ are singular close to both triple points and corresponding inner solutions are needed to describe details of the flows near these points.

Figures 3 and 4 depict the shapes of the free surfaces near the triple point, which are predicted by the second-order outer solution. See Appendix B for the details of the calculations of these shapes. In Fig. 3, the black line corresponds to the first-order shape of the left free surface, $\frac{1}{2}\epsilon t^2 \varphi_{0,y}^{-}(x, 1)$, the purple line corresponds to the regular part of
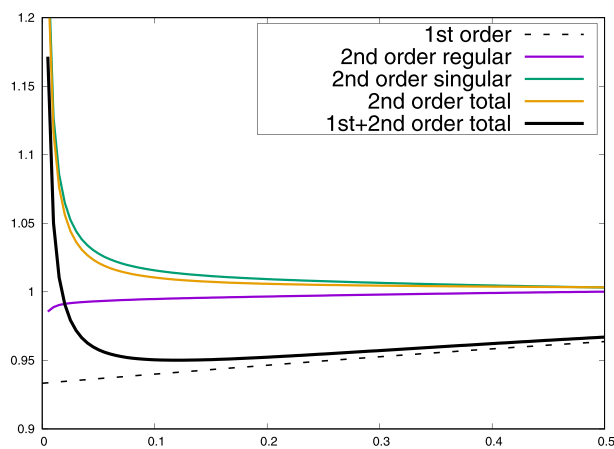

FIG. 4. The shape of the right free surface in the dimensionless variables for $\gamma = 0.5$, $t = 1$, and $\epsilon = 0.4$.
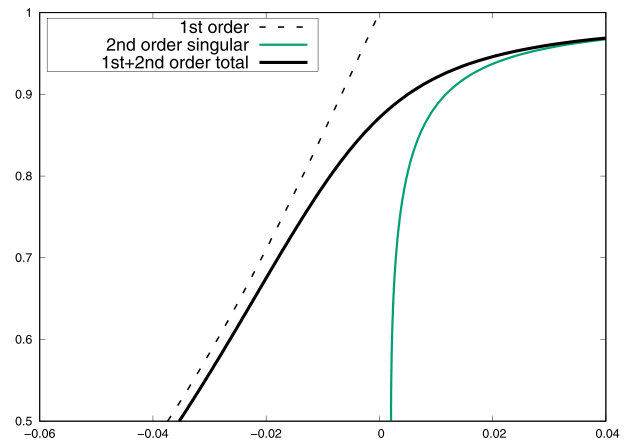
the second-order shape, $\frac{1}{24}\epsilon^2 t^4 [\phi_{R0,y}(x, 1) + \phi_{R1,y}^{-}(x, 1)]$, the green line corresponds to the singular part of the second-order shape, $\frac{1}{24}\epsilon^2 t^4 \phi_{s,y}^{-}(x, 1)$, the red line corresponds to the total second-order shape, and the yellow line corresponds to the shape provided by both the first and second shape components. The lines are shown with respect to the initial position of the left free surface, $y = 1$. The definition of the lines in Fig. 4 is exactly the same as for Fig. 3 except that the superscript "−" for the potentials should be replaced by "+" and the word "left" by "right." The value of ϵ in Figs. 3 and 4 is relatively high, which corresponds to the larger times than anticipated for an early stage. Close to the edge of the left free surface, $x = 0$, the second-order solution becomes as important as the leading-order one. That implies that the original expansions (13) become invalid near the upper triple point $(0, 1)$. Hence, an inner region and the corresponding inner solution are required there. The size of the inner region depends on the small parameter ϵ and tends to zero as $\epsilon \to 0$. In our problem, $\rho^- < \rho^+$ and the free surface of the left lighter fluid are expected to go upward near the triple point, as predicted by the leading-order solution. However, the second-order solution predicts that the left free surface goes down near the triple point, see Fig. 3. A similar problem is observed in Fig. 4 for the right free surface. These difficulties are resolved by introducing the inner solution.

Figure 5 shows the shape of the interface and the contribution of the leading-order and the second-order singular components. In Fig. 5, the black line corresponds to the first-order shape of the interface, $\frac{1}{2}\epsilon t^2 \varphi_{0,x}^{+}(0, y)$, the green line corresponds to the singular part of the second order shape, $\frac{1}{24}\epsilon^2 t^4 \phi_{s,x}^{\pm}(0, y)$, and the yellow line corresponds to the shape provided by both the first and second shape components.

The flow close to the point bottom $(0, 0)$ is investigated in Sec. V, and the local flow close to the upper triple point $(0, 1)$ is studied in Sec. VI.

V. THE INNER SOLUTION NEAR THE BOTTOM TRIPLE POINT

The leading-order solution (17) and (18) is not valid near the point $(0, 0)$, where the fluid interface meets the bottom. At this point,

20 February 2024 12:34:50

the horizontal velocity of the interface exhibits a logarithmic singularity

$$\varphi_{0,x}^{\pm}(0,y) = \frac{2}{\pi}\delta\log\left(\tan\frac{\pi y}{4}\right).$$

The size of small vicinity of the point (0, 0) is unknown in advance and should be determined using the matching conditions between the outer second-order solution (13) and the corresponding inner solution. We only know that this size tends to zero as $\epsilon \to 0$. We introduce the size of the inner region $a(\epsilon)$, where $a(\epsilon) \to 0$ as $\epsilon \to 0$, and the inner variables, ξ, η by $x = a(\epsilon)\xi$, $y = a(\epsilon)\eta$. Then the potentials $\varphi_0^{\pm}$, near the intersection point within the stretched inner variables ξ and η, behave like

$$\varphi_0^+ = \delta\left(1 + \frac{2}{\pi}\xi a\log a + \frac{2}{\pi}a\xi\left(\log\rho + \log\frac{\pi}{4} - 1\right) - \frac{2}{\pi}a\eta\theta\right)$$
$$+ \mathrm{O}\left(\frac{a}{\log a}\right),$$
$$\varphi_0^- = \delta\left(-1 + \frac{2}{\pi}\xi a\log a + \frac{2}{\pi}a\xi\left(\log\rho + \log\frac{\pi}{4} - 1\right) - \frac{2}{\pi}a\eta\theta\right)$$
$$+ \mathrm{O}\left(\frac{a}{\log a}\right), \tag{37}$$

where $\rho = (\xi^2 + \eta^2)^{1/2}$, $\theta = \arctan(\eta/\xi)$, and $0 < \theta < \pi/2$ for the right fluid and $\pi/2 < \theta < \pi$ for the left fluid. To derive Eq. (37), the values of the first-order potentials at the bottom corner point, $\varphi_0^{\pm}(0,0) = \pm\delta$, were used.

Equations (25) and (26) provide the asymptotic behavior of the second-order outer solution near the point (0, 0). The first terms in (25) and (26) contain the singular behavior of $\varphi_1^{\pm}$ at (0, 0) and the second terms, $\phi^{\pm}$, are regular at the bottom corner point. Hence, the asymptotic behavior of the second-order potentials near (0, 0) is

$$\frac{1}{6}\epsilon t^3\varphi_1^+ = \frac{t^3}{6}\left(\frac{-a}{\log a}\right)\frac{2+\gamma}{1+\gamma}\frac{4\delta^2}{\pi^2}\left[-\log^2 a - 2\log a\log\frac{\pi\rho}{4}\right] + \mathrm{O}\left(\frac{a}{\log a}\right)$$
$$= \frac{4t^3\delta^2}{6\pi^2}\frac{2+\gamma}{1+\gamma}\left(a\log a + 2a\log\frac{\pi\rho}{4}\right) + \mathrm{O}\left(\frac{a}{\log a}\right), \tag{38}$$

$$\frac{1}{6}\epsilon t^3\varphi_1^- = \frac{t^3}{6}\left(\frac{-a}{\log a}\right)\frac{1+2\gamma}{1+\gamma}\frac{4\delta^2}{\pi^2}\left[-\log^2 a - 2\log a\log\frac{\pi\rho}{4}\right] + \mathrm{O}\left(\frac{a}{\log a}\right)$$
$$= \frac{4t^3\delta^2}{6\pi^2}\frac{1+2\gamma}{1+\gamma}\left(a\log a + 2a\log\frac{\pi\rho}{4}\right) + \mathrm{O}\left(\frac{a}{\log a}\right). \tag{39}$$

To determine the size $a(\epsilon)$ of the inner region, the terms (37) are compared with terms (38) and (39). It is seen that the first- and second-order terms in the asymptotic expansion (13) are of the same order if and only if

$$a = -\epsilon\log a. \tag{40}$$

Equation (40) is the same as Eq. (57) in Ref. 16. The analysis below extends that of Ref. 16, where the local analysis is performed for the classical dam break problem.

We also need the asymptotic behavior of the interface, $x = \epsilon X(y, t)$, near the bottom corner point, see (13) and (20),

$$a\xi = \epsilon\frac{t^2}{2}\frac{2}{\pi}\delta\log\left(\frac{\pi}{4}a\eta\right),$$
$$\xi = -\frac{t^2}{\pi}\delta - \frac{t^2}{\pi}\delta\log\frac{\pi\eta}{4}\frac{1}{\log a} + \mathrm{O}\left(\frac{1}{\log^2 a}\right), \tag{41}$$

as $a \to 0$.

The asymptotic formulas (37)–(41) suggest the following expansions for the inner velocity potentials $\varphi_i^{\pm}(\xi,\eta,t,\epsilon)$ and for the shape of the interface close to the bottom

$$\varphi_i^+ = t\delta + a\log a\Phi_{i0}^+(\xi,\eta,t) + a\Phi_{i1}^+(\xi,\eta,t) + \mathrm{O}\left(\frac{a}{\log a}\right), \tag{42}$$

$$\varphi_i^- = -t\delta + a\log a\Phi_{i0}^-(\xi,\eta,t) + a\Phi_{i1}^-(\xi,\eta,t) + \mathrm{O}\left(\frac{a}{\log a}\right), \tag{43}$$

$$\xi = -\frac{t^2}{\pi}\delta - \frac{1}{\log a}H(\eta,t) + \mathrm{O}\left(\frac{1}{\log^2 a}\right). \tag{44}$$

The function $X(y,t,\epsilon)$, which describes the shape of the interface, see the kinematic boundary condition (9), is now given as

$$X = \frac{t^2}{\pi}\delta\log a + H(\eta,t) + O\left(\frac{1}{\log a}\right). \tag{45}$$

The potentials ϕ_{i0}^+, ϕ_{i1}^+ and ϕ_{i0}^-, ϕ_{i1}^- satisfy the Laplace equations in $\eta > 0$, $\xi > -\delta t^2/\pi$ and $\xi < -\delta t^2/\pi$ correspondingly. Substituting (42)–(44) in Eqs. (8) and (9), we obtain the kinematic conditions at the leading and second orders

$$\frac{2t}{\pi}\delta = \Phi_{i0,\xi}^+ = \Phi_{i0,\xi}^-, \tag{46}$$

$$H_t = -\Phi_{i0,\xi\xi}^+ H + \Phi_{i1,\xi}^+ + H_n\Phi_{i0,\eta}^+ = -\Phi_{i0,\xi\xi}^- H + \Phi_{i1,\xi}^- + H_n\Phi_{i0,\eta}^-, \tag{47}$$

and the dynamic conditions

$$\Phi_{i0,t}^+ - \gamma\Phi_{i0,t}^- = -\frac{1}{2}\left(\gamma|\nabla\Phi_{i0}^-|^2 - |\nabla\Phi_{i0}^+|^2\right), \tag{48}$$

$$\Phi_{i1,t}^+ - \gamma\Phi_{i1,t}^- - H(\Phi_{i0,t\xi}^+ - \gamma\Phi_{i0,t\xi}^-) + \eta(1-\gamma)$$
$$= -\gamma\left(\Phi_{i0,\xi}^-\Phi_{i1,\xi}^- + \Phi_{i0,\eta}^-\Phi_{i1,\eta}^- - H\Phi_{i0,\xi}^-\Phi_{i0,\xi\xi}^- - H\Phi_{i0,\eta}^-\Phi_{i0,\eta\xi}^-\right)$$
$$+ \Phi_{i0,\xi}^+\Phi_{i1,\xi}^+ + \Phi_{i0,\eta}^+\Phi_{i1,\eta}^+ - H\Phi_{i0,\xi}^+\Phi_{i0,\xi\xi}^+ - H\Phi_{i0,\eta}^+\Phi_{i0,\eta\xi}^+, \tag{49}$$

at the interface $\xi = -\delta t^2/\pi$ in the leading $O(a\log a)$ and the second $O(a)$ orders as $a \to 0$. The bottom boundary condition (10) is to be satisfied by the potentials $\Phi_{i0}^{\pm}$ and $\Phi_{i1}^{\pm}$ at $\eta = 0$.

Moreover, the unknown functions $\Phi_{i0}^{\pm}(\xi,\eta,t)$ are to be matched with the inner limits of the outer solutions defined by (37), (39), and (40). The matching conditions at leading order are

$$\Phi_{i0}^+(\xi,\eta,t) = \frac{2t}{\pi}\xi\delta + \frac{4t^3\delta^2}{6\pi^2}\frac{2+\gamma}{1+\gamma} + o(1), \quad \rho \to \infty, \tag{50}$$

$$\Phi_{i0}^-(\xi,\eta,t) = \frac{2t}{\pi}\xi\delta + \frac{4t^3\delta^2}{6\pi^2}\frac{1+2\gamma}{1+\gamma} + o(1), \quad \rho \to \infty. \tag{51}$$

The functions on the right-hand sides in (50) and (51) are solutions of the inner problem in the leading order as $a \to 0$ because they satisfy the Laplace equations, the conditions (46) and (48) at the interface, and the condition (10) on the bottom.

20 February 2024 12:34:50

The boundary value problem for the second-order inner potentials $\phi_{i1}^{\pm}(\xi, \eta, t)$ is more complicated than the one for the first-order inner potentials. The kinematic and dynamic interface conditions follow from (47) and (49), respectively, as

$$\Phi_{i1,\xi}^{+} = \Phi_{i1,\xi}^{-} = H_t, \tag{52}$$

$$\Phi_{i1,t}^{+} - \gamma \Phi_{i1,t}^{-} - \frac{2t\delta}{\pi}(\Phi_{i1,\xi}^{+} - \gamma \Phi_{i1,\xi}^{-}) - \frac{2\delta}{\pi}(1-\gamma)H + \eta(1-\gamma) = 0. \tag{53}$$

The interface conditions are imposed at $\xi = -\delta t^2/\pi$. The function Φ_{i1}^{+} is harmonic in the flow region $\xi > -\delta t^2/\pi$, and the function Φ_{i1}^{-} is harmonic in the flow region $\xi < -\delta t^2/\pi$. The functions $\Phi_{i1}^{\pm}$ should also satisfy the slip boundary conditions at $\eta = 0$. The functions $\Phi_{i1}^{\pm}$ and $H(\eta, t)$ should be matched with the outer solution (38), (39), and (41). The matching conditions read

$$\Phi_{i1}^{+} = \Phi_{i\infty}^{+} + o(1), \tag{54}$$

$$\Phi_{i1}^{-} = \Phi_{i\infty}^{-} + o(1), \tag{55}$$

$$H(\eta, t) = \frac{t^2}{\pi}\delta \log \frac{\pi\eta}{4} + o(1), \tag{56}$$

as $\rho \to \infty$, where

$$\Phi_{i\infty}^{+} = \delta t \left(\frac{2}{\pi}\xi \left(\log \rho + \log \frac{\pi}{4} - 1 \right) - \frac{2}{\pi}\eta\theta \right) + \frac{4t^3\delta^2}{3\pi^2}\frac{2+\gamma}{1+\gamma}\log\frac{\pi\rho}{4}, \tag{57}$$

$$\Phi_{i\infty}^{-} = \delta t \left(\frac{2}{\pi}\xi \left(\log \rho + \log \frac{\pi}{4} - 1 \right) - \frac{2}{\pi}\eta\theta \right) + \frac{4t^3\delta^2}{3\pi^2}\frac{1+2\gamma}{1+\gamma}\log\frac{\pi\rho}{4}, \tag{58}$$

and θ is defined in (37). The functions $\Phi_{i\infty}^{\pm}$ given by (57) and (58) are harmonic and satisfy the bottom boundary condition, but are singular at $\xi = 0, \eta = 0$, which is a point inside the flow domain of $\Phi_{i1}^{+}(\xi, \eta, t)$.

Let us introduce the new variables x_1 and y_1 as

$$\xi = -\frac{\delta t^2}{\pi} - y_1, \quad \eta = x_1$$

and continue the new unknown functions $\phi^{\pm}(x_1, y_1, t) = \Phi_{i1}^{\pm}(-\delta t^2/\pi - y_1, x_1, t)$ and $h(x_1, t) = -H(x_1, t)$ symmetrically with respect to the bottom line $x_1 = 0$. The kinematic and dynamic interface conditions (52) and (53) in the new variables become

$$\phi_{y_1}^{+} = \phi_{y_1}^{-} = h_t, \quad \phi_t^{+} - \gamma \phi_t^{-} + \frac{2\delta}{\pi}(1-\gamma)h + (1-\gamma)|x_1| = 0, \tag{59}$$

at $y_1 = 0, -\infty < x_1 < \infty$, which provides the boundary condition

$$\phi_{tt}^{+} - \gamma \phi_{tt}^{-} + \frac{2\delta}{\pi}(1-\gamma)\phi_{y_1}^{+} = 0, \quad (y_1 = 0, -\infty < x_1 < \infty). \tag{60}$$

The condition (60) should be considered together with the initial conditions

$$\phi^{+}(x_1, 0, 0) = 0, \quad \phi^{-}(x_1, 0, 0) = 0,$$
$$\phi_t^{+}(x_1, 0, 0) - \gamma\phi_t^{-}(x_1, 0, 0) = -(1-\gamma)|x_1|, \tag{61}$$

which follow from (12). The potential $\phi^{+}(x_1, y_1, t)$ satisfies Laplace's equation in the half plane $y_1 < 0$, and the potential $\phi^{-}(x_1, y_1, t)$ satisfies

Laplace's equation in the half plane $y_1 > 0$. They should satisfy the far-field conditions (54) and (55),

$$\phi^{+}(x_1, y_1, t) = \Phi_{i\infty}^{+}\left(-\frac{\delta t^2}{\pi} - y_1, x_1, t\right) + o(1), \tag{62}$$

$$\phi^{-}(x_1, y_1, t) = \Phi_{i\infty}^{-}\left(-\frac{\delta t^2}{\pi} - y_1, x_1, t\right) + o(1), \tag{63}$$

as $\rho \to \infty$. The functions $\phi^{\pm}$ satisfy the slip boundary condition at $x_1 = 0$, which follows from the definition of these functions. See Fig. 6 for the problem for $\phi^{\pm}$.

The forcing in the derived initial boundary-value problem for the potentials ϕ^{+} and ϕ^{-} comes from the initial conditions (61) and far-field conditions (62) and (63). This problem is similar to the Cauchy–Poisson problem for internal waves on the interface between two semi-infinite fluids in the "gravity" field with gravitational acceleration being equal to $2\delta/\pi$. It is convenient to decompose the potentials $\phi^{\pm}$ as

$$\phi^{+}(x_1, y_1, t) = \phi_{\infty}^{+}(x_1, y_1, t) + \psi^{+}(x_1, y_1, t), \tag{64}$$

$$\phi^{-}(x_1, y_1, t) = \phi_{\infty}^{-}(x_1, y_1, t) + \psi^{-}(x_1, y_1, t), \tag{65}$$

where the potentials $\phi_{\infty}^{\pm}(x_1, y_1, t)$ satisfy Laplace's equation and the far-field conditions. The functions $\Phi_{i\infty}^{\pm}(-\frac{\delta t^2}{\pi} - y_1, x_1, t)$ in (62) and (63) satisfy Laplace's equation, but the function $\Phi_{i\infty}^{+}(x_1, y_1, t)$ is singular at the point $x_1 = 0, y_1 = -\delta t^2/\pi$, which is inside the flow region $y_1 < 0$. See Ref. 16 for more discussions.

To avoid singularities of the potentials ϕ_{∞}^{-} and ϕ_{∞}^{+} in the regions, where they are defined, we use the technique from Ref. 16. To construct $\phi_{\infty}^{-}(x_1, y_1, t)$, we introduce a new polar coordinate system with the origin at $x_1 = 0, y_1 = -\beta t^2$,

$$x_1 = r\cos\bar\theta, y_1 = -\beta t^2 + r\sin\bar\theta, \tag{66}$$

where β is an undetermined positive constant. We substitute (66) in the right-hand side of (63) and find asymptotic behavior of $\Phi_{i\infty}^{-}(-\frac{\delta t^2}{\pi} + \beta t^2 + r\sin\bar\theta, r\cos\bar\theta, t)$ as $r \to \infty$ neglecting terms, which tend to zero as $r \to \infty$. The resulting function, which satisfies Laplace equation and the matching condition (63) in the far field, is
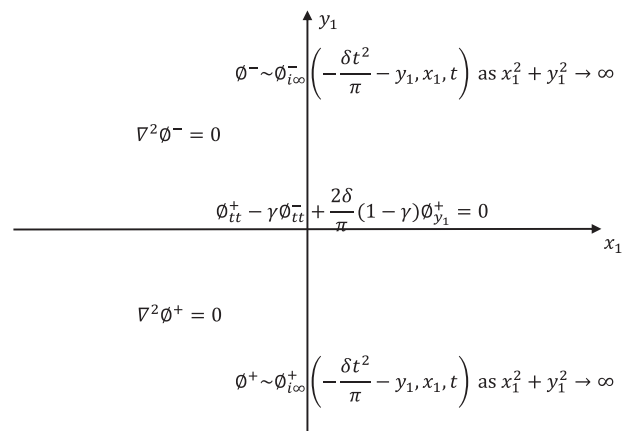

FIG. 6. The boundary value problem for $\phi^{\pm}$.

taken as $\phi_\infty^-(x_1, y_1, t)$ in (65). This function is regular in $y_1 \geq 0$. Now, we rewrite the potential ϕ_∞^- using the polar coordinate system (66) and Eq. (58) as

$$\phi_\infty^-(x_1, y_1, t)$$
$$= \frac{2\delta t}{\pi}\left(-\frac{\delta^2 t^2}{3\pi}\log\frac{\pi r}{4} - y_1 \log\frac{\pi r}{4} + y_1 - x_1\left(\bar{\theta} - \frac{\pi}{2}\right) + \beta t^2\right).$$

Similarly, to construct $\phi_\infty^+(x_1, y_1, t)$, we introduce another coordinate system whose center is outside the domain, $y_1 < 0$,

$$x_1 = \tilde{r}\cos\tilde{\theta}, y_1 = \tilde{r}\sin\tilde{\theta} + \alpha t^2, \quad \alpha > 0. \quad (67)$$

We need this second coordinate system to resolve the singularity in ϕ_∞^+. Using Eqs. (57) and (67), we find that

$$\phi_\infty^+(x_1, y_1, t)$$
$$= \frac{2\delta t}{\pi}\left(\frac{\delta^2 t^2}{3\pi}\log\frac{\pi\tilde{r}}{4} - y_1\log\frac{\pi\tilde{r}}{4} + y_1 - x_1\left(\tilde{\theta} + \frac{\pi}{2}\right) - \alpha t^2\right).$$

The kinematic boundary condition at the interface, first equation in (59), together with the decomposed potentials (64) and (65) provides

$$\frac{2\delta t}{\pi}\left[-\log\left(\frac{\pi}{4}\sqrt{x_1^2 + \alpha^2 t^4}\right) - \frac{\delta^2 t^2}{3\pi}\frac{\alpha t^2}{x_1^2 + \alpha^2 t^4} + \frac{\alpha^2 t^4}{x_1^2 + \alpha^2 t^4}\right] + \psi_{y_1}^+$$
$$= \frac{2\delta t}{\pi}\left[-\log\left(\frac{\pi}{4}\sqrt{x_1^2 + \beta^2 t^4}\right) - \frac{\delta^2 t^2}{3\pi}\frac{\beta t^2}{x_1^2 + \beta^2 t^4} + \frac{\beta^2 t^4}{x_1^2 + \beta^2 t^4}\right]$$
$$+ \psi_{y_1}^- = h_t, \quad (y_1 = 0). \quad (68)$$

By decomposing the function $h(x_1, t)$ as

$$h(x_1, t) = -\frac{\delta t^2}{\pi}\log\left(\frac{\pi}{4}\sqrt{x_1^2 + \alpha^2 t^4}\right) + \bar{h}(x_1, t), \quad (69)$$

we rewrite the Eq. (68) as

$$\bar{h}_t - \psi_{y_1}^+ = \frac{2\alpha\delta}{\pi}\frac{t^5}{x_1^2 + \alpha^2 t^4}\left(2\alpha - \frac{\delta^2}{3\pi}\right). \quad (70)$$

The dynamic boundary condition at the interface, second equation in (59), together with the Eqs. (64) and (65) provides

$$\psi_t^+ - \gamma\psi_t^- + \frac{2\delta}{\pi}(1 - \gamma)\bar{h}$$
$$= (x_1 - |x_1|)(1 - \gamma) + \frac{2\delta}{\pi}x_1(\tilde{\theta} - \gamma\bar{\theta}) - 2\gamma\frac{\delta^3 t^2}{\pi^2}\log\left(\frac{r}{\tilde{r}}\right)$$
$$+ \frac{2\delta}{\pi}t^2(\alpha + \gamma\beta) + 4\delta\alpha^2\frac{t^6}{\pi\tilde{r}^2}\left(\alpha - \frac{\delta^2}{3\pi}\right) + 4\delta\gamma\beta^2\frac{t^6}{\pi r^2}\left(\beta - \frac{\delta^2}{3\pi}\right). \quad (71)$$

To simplify the boundary conditions (70) and (71), we set $\alpha = \beta = \frac{\delta^2}{3\pi}$. Then, conditions (70) and (71) combined together yield

$$\psi_{tt}^+ - \gamma\psi_{tt}^- + \frac{2\delta}{\pi}(1 - \gamma)\psi_{y_1}^+ = -\frac{8\delta^6}{3\pi^2}(1 - \gamma)\frac{t^5}{\delta^4 t^4 + 9\pi^2 x_1^2}. \quad (72)$$

The initial conditions are obtained as

$$\psi^+(x_1, 0, 0) = 0, \quad \psi^-(x_1, 0, 0) = 0,$$
$$\psi_t^+ - \gamma\psi_t^- = 0, \quad y_1 = 0, t = 0. \quad (73)$$

Hence, we have obtained the following boundary value problem:

$$\nabla^2\psi^+ = 0, \quad y_1 < 0, \quad \nabla^2\psi^- = 0, \quad y_1 > 0,$$
$$\psi_{tt}^+ - \gamma\psi_{tt}^- + \frac{2\delta}{\pi}(1 - \gamma)\psi_{y_1}^+ = -\frac{8\delta^6}{3\pi^2}(1 - \gamma)\frac{t^5}{\delta^4 t^4 + 9\pi^2 x_1^2}, \quad (74)$$
$$y_1 = 0, \quad \psi^+(x_1, 0, 0) = 0, \quad \psi^-(x_1, 0, 0) = 0,$$
$$\psi_t^+ - \gamma\psi_t^- = 0, \quad y_1 = 0, t = 0, \quad \psi^\pm \to 0(x_1^2 + y_1^2 \to \infty).$$

The linear problem (74) is equivalent to an unsteady problem of two unbounded fluids with external pressure at the interface. The Fourier transform in x_1 applied to the boundary value problem (74) gives

$$\Psi^+ = c_1(t, \omega)e^{|\omega|y_1}, \quad y_1 < 0, \quad \Psi^- = c_2(t, \omega)e^{-|\omega|y_1}, \quad y_1 > 0,$$
$$c_{1,tt} - \gamma c_{2,tt} + \frac{2\delta}{\pi}(1 - \gamma)|\omega|c_1 = -\frac{8\delta^4}{9\pi^3}t^3\sqrt{\frac{\pi}{2}}(1 - \gamma)e^{-|\omega|\frac{\delta^2 t^2}{3\pi}}, \quad (75)$$
$$c_1(0, \omega) = 0, \quad c_2(0, \omega) = 0, \quad c_{1,t}(0, \omega) - \gamma c_{2,t}(0, \omega) = 0,$$

where Ψ^+ is the Fourier transform of ψ^+, Ψ^- is of ψ^-, and ω is the parameter of the Fourier transform. There are two unknowns $c_1(t, \omega)$ and $c_2(t, \omega)$ in the differential Eq. (75). Another equation comes from the kinematic condition (68)

$$c_1(t, \omega) = -c_2(t, \omega). \quad (76)$$

Hence, using (75) and (76), we obtain

$$c_1(t, \omega) = -\frac{4\delta^4}{9\pi^2\sqrt{|\omega|}}\int_0^t \tau^3 e^{-|\omega|\frac{\delta^2\tau^2}{3\pi}}\sin\left(\sqrt{\frac{2|\omega|}{\pi}}\delta(t - \tau)\right)d\tau. \quad (77)$$

From the dynamic boundary condition (71), we obtain the shape of the interface

$$\bar{h}(x_1, t) = -\frac{\pi}{2\delta}\frac{\psi_t^+ - \gamma\psi_t^-}{1 - \gamma} + x_1\frac{\tilde{\theta} - \gamma\bar{\theta}}{1 - \gamma} + \frac{\delta t^2}{3\pi}. \quad (78)$$

In (78), $y_1 = 0$, $\tilde{\theta} = -\bar{\theta}$ and $\psi_t^+ = -\psi_t^-$. Using the inverse Fourier transform and then taking the time derivative of $\psi^\pm$ at $y_1 = 0$, we get

$$\psi_t^+(x_1, 0, t) = -\frac{8\delta^5}{9\pi^3}\int_0^\infty \cos(\omega x_1)\int_0^t s^3 e^{-\omega\frac{\delta^2 s^2}{3\pi}}\cos\left(\delta\sqrt{\frac{2\omega}{\pi}}(t - s)\right)ds\,d\omega.$$

To simplify the above equation, the integration variable of the improper integral is changed from ω to τ by $\omega = \frac{\pi\tau^2}{2\delta^2 t^2}$ and the inner integral variable is changed from s to τ_0 by $s = t\tau_0/\tau$,

$$\psi_t^+(x_1, 0, t) = -\frac{8\delta^3 t^2}{3\pi^2}\int_0^\infty \frac{\cos\left(\frac{u\pi\tau^2}{2}\right)}{\tau^3}B(\tau)d\tau, \quad (79)$$

where

$$B(\tau) = e^{-\tau^2/6}(3 - \tau^2) - 3\cos\tau, \quad (80)$$

and $u = x_1/(\delta^2 t^2)$. Equations (44) and (78)–(80) provide the shape of the interface in the inner region as

$$x = x_*(t) + \epsilon t^2 \delta G(u), \quad x_*(t) = \frac{1}{\pi}\epsilon\delta t^2\log(a(\epsilon)\delta^2 t^2), \quad (81)$$

$$G(u) = \frac{1}{\pi}\log\left(\frac{\pi}{4}\sqrt{u^2+\frac{1}{9\pi^2}}\right) + u\arctan\left(\frac{1}{3\pi u}\right) - \frac{1}{3\pi} - \frac{3\pi}{2}S(u) \tag{82}$$

$$S(u) = \frac{8}{9\pi^2}\int_0^\infty B(\tau)\cos\left(\frac{\pi}{2}\tau^2 u\right)\frac{d\tau}{\tau^3}.$$

The function $S(u)$ given by (82) was introduced in Ref. 16, see Eq. (83) there. The function $G(u)$ appeared in the formula (84) of Ref. 16 for the corresponding shape of the inner free surface near the bottom point where $\delta = 1$. Note the misprint in Eq. (84) of Ref. 16, where the factor three in front of $S(u)$ in the formula for $G(u)$ is missing. The head of the interface moves along the bottom as

$$x = x_0(t) = x_*(t) + \epsilon t^2 \delta G(0),$$

where $G(0) = -\frac{1}{\pi}\log(12) - \frac{1}{3\pi} - \frac{3\pi}{2}S(0) \approx -0.9918$. In the moving self-similar variables $(x-x_0(t))/(\epsilon t^2\delta)$ and $u = y/(a\delta^2 t^2)$, the shape of the interface does not depend on any parameters including the density ratio γ. We have

$$\frac{x-x_0(t)}{\epsilon t^2\delta} = G(u) - G(0). \tag{83}$$

The function $G(u) - G(0)$ is shown in Fig. 7. The shape of the interface for a certain values of ϵ, δ, and time t is obtained by stretching the curve in Fig. 7 by $a(\epsilon)\delta^2 t^2$ in the vertical direction, then by $\epsilon\delta t^2$ in the horizontal direction, and finally shifting by $x_0(t)$ in the horizontal direction. We note different stretching in the vertical and horizontal directions in terms of ϵ and δ but not in terms of time. The shapes of the interface for different γ, $t = 1$ and $\epsilon = 0.1$ are shown in Fig. 8.

It can be shown that $\partial x_0/\partial\delta < 0$ for small ϵt^2 and $0 < \delta \leq 1$, and $x_0 = 0$ for $\delta = 0$. Therefore, $x_0(t)$ is negative for $0 < \delta \leq 1$, the interface moves toward the lighter fluid, and monotonically decreases as δ increases.

The tangent of the angle between the tangent to the interface at the bottom triple point and the positive x axis is obtained using (83) and the definition of the variable u as

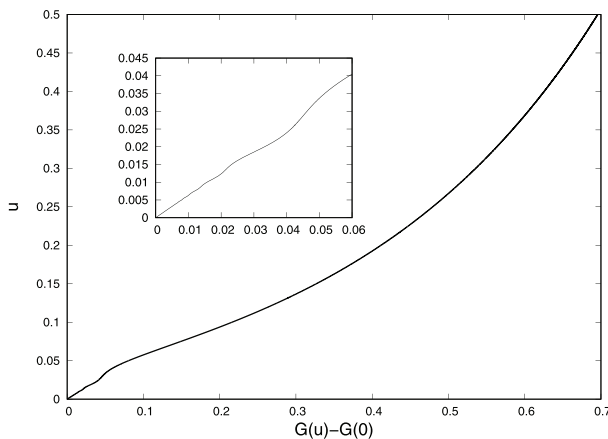$$\frac{dy}{dx} = \frac{2}{\pi}\delta\log\left(\frac{1}{a(\epsilon)}\right),$$

FIG. 7. The shape of the interface close to the bottom in the self-similar variables.
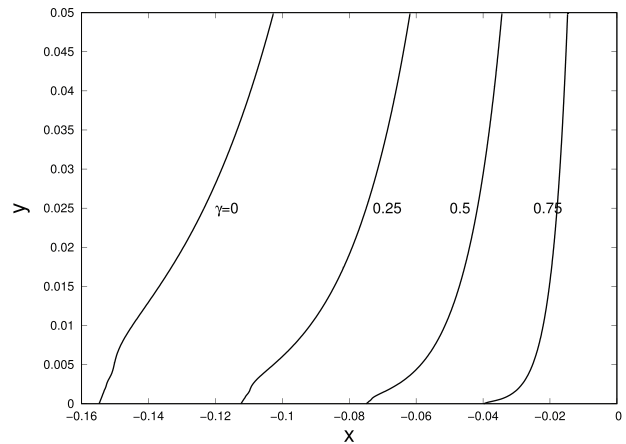

FIG. 8. The shape of the interface close to the bottom point (0, 0) in the dimensionless variables by the leading-order inner solution, for $t = 1.0$, $\epsilon = 0.1$, and for γ values 0, 0.25, 0.5, and 0.75 from left to right, respectively.

where $a(\epsilon)$ is defined by (40) and it was used that $S'(0) = 0$ and $G'(0) = \pi/2$. It is seen that the angle decreases with decrease in δ, which is with increase in the density of the lighter fluid.

VI. THE INNER REGION NEAR THE UPPER TRIPLE POINT

As it is shown in Fig. 2, first-order outer solution predicts a jump discontinuity in the free surface at the point (0, 1). The relative jump of the free surface is δt^2 with the heavier fluid moving down and the lighter one moving up. Second-order outer solution has been derived in Sec. IV, but due to the singular nature of the second-order vertical velocity at this triple point, see Eq. (33), it is unable to properly capture the behavior of the fluid near the triple point (0, 1) where the horizontal free surfaces and the interface originally meet. An inner region solution is required near this point.

First-order velocities of the interface are given by (20). Using (20), the asymptotic behavior of the vertical and horizontal velocities near the triple point are found as

$$\varphi_{0,y}^\pm = \mp\delta + \delta x + O(x^2), \quad y = 1, \quad x \to 0^\pm, \tag{84}$$

$$\varphi_{0,x}^\pm = -\delta + \delta y + O(y^2), \quad x = 0, \quad y \to 1^-. \tag{85}$$

It is seen that the velocities are continuous in the regions $x > 0$ and $x < 0$, but discontinuous at $x = 0$. By introducing the inner variables (ξ, η) by

$$x = \xi\epsilon t^2, \quad y - 1 = \eta\epsilon t^2, \tag{86}$$

where $\xi = O(1)$, $\eta = O(1)$, and then using the behavior of the flow velocity near the triple point together with (17)–(20), we determine the asymptotic behavior of the leading-order outer velocity potential

$$\varphi_0^+(\epsilon t^2\xi, 1 + \epsilon t^2\eta) = -\delta\eta\epsilon t^2 + O(\epsilon^2), \tag{87}$$

$$\varphi_0^-(\epsilon t^2\xi, 1 + \epsilon t^2\eta) = \delta\eta\epsilon t^2 + O(\epsilon^2), \tag{88}$$

as $\epsilon \to 0$.

To find the asymptotic behavior of the second-order outer solution near the triple, Eqs. (25), (26), (31), and (32) are used with the result

$$\varphi_1^+(\epsilon t^2 \xi, 1 + \epsilon t^2 \eta) = \frac{2+\gamma}{1+\gamma}\delta^2 + \frac{\Gamma}{2\pi}\theta + b^+ + o(1), \quad (89)$$

$$\varphi_1^-(\epsilon t^2 \xi, 1 + \epsilon t^2 \eta) = \frac{1+2\gamma}{1+\gamma}\left(\delta^2(1 + a\xi)^2 - a^2\delta^2\eta^2\right)$$
$$+ \frac{\Gamma}{2\pi}\theta + b^- + o(1), \quad (90)$$

where $\theta = \arctan(\eta/\xi)$ and $\pi < \theta < \frac{3}{2}\pi$ in the light fluid and $\frac{3}{2}\pi < \theta < 2\pi$ in the heavier fluid. The constants Γ, b^+, and b^- are given by (32) as functions of the density ratio γ. Then, using expansions (13) and asymptotic formulas (87)–(90), we arrive at the asymptotic behavior of the velocity potentials, free surfaces, and the interface in the main flow region close to the triple point

$$\varphi^+ = \epsilon t^3\left\{-\delta\eta + \frac{1}{6}\frac{2+\gamma}{1+\gamma}\delta^2 + \frac{\Gamma}{12\pi}\theta + \frac{1}{6}b^+\right\} + O(\epsilon^2), \quad (91)$$

$$\varphi^- = \epsilon t^3\left\{\delta\eta + \frac{1}{6}\frac{1+2\gamma}{1+\gamma}\delta^2 + \frac{\Gamma}{12\pi}\theta + \frac{1}{6}b^-\right\} + O(\epsilon^2), \quad (92)$$

$$Y^+ = -\frac{1}{2}\delta t^2 + \frac{1}{24}t^4\frac{\Gamma}{2\pi}\frac{1}{\xi t^2} + o(1), \quad (93)$$

$$Y^- = \frac{1}{2}\delta t^2 + \frac{1}{24}t^4\frac{\Gamma}{2\pi}\frac{1}{\xi t^2} + o(1), \quad (94)$$

$$X = -\frac{\Gamma}{48\pi}\frac{t^2}{\eta} + o(1), \quad (95)$$

as $\epsilon \to 0$.

Asymptotic formulas (91)–(95) suggest the following forms for the inner velocity potentials $\varphi_i^\pm(\xi, \eta, t, \epsilon)$, the free surface shapes, $\eta = \eta^\pm(\xi, t)$, and the interface shape $\xi = \xi_i(\eta, t)$,

$$\varphi_i^\pm(\xi, \eta, t, \epsilon) = \epsilon t^3 \phi_i^\pm\left(\frac{x}{\epsilon t^2}, \frac{y-1}{\epsilon t^2}\right) + O(\epsilon^2), \quad (96)$$

$$\eta^\pm(\xi, t) = \mp\frac{\delta}{2} + B_1^\pm(\xi) + o(1), \quad (97)$$

$$\xi_i(\eta, t) = H_1(\eta) + o(1). \quad (98)$$

The functions $Y^\pm(x, t, \epsilon)$ and $X(y, t, \epsilon)$, which describe the shapes of the horizontal and vertical free surfaces in the boundary conditions (6)–(11), are now given as

$$Y^\pm(x, t, \epsilon) = \mp\frac{\delta t^2}{2} + t^2 B_1^\pm(\xi) + o(1), \quad (99)$$

$$X(y, t, \epsilon) = t^2 H_1(\eta) + o(1). \quad (100)$$

Substituting (96), (99), and (100) in (5)–(12) provides the following conditions at the free surfaces and the interface in the leading order as $\epsilon \to 0$ in the inner variables

$$3\phi_i^\pm - 2\xi\phi_{i,\xi}^\pm - 2\eta\phi_{i,\eta}^\pm = -\frac{1}{2}|\nabla\phi_i^\pm|^2 \pm \frac{1}{2}\delta - B_1^\pm(\xi),$$
$$\text{at } \eta = \mp\frac{\delta}{2} + B_1^\pm(\xi), \quad (101)$$

$$-2\xi B_{1,\xi}^\pm + (\mp)\delta + 2B_1^\pm = \phi_{i,\eta}^\pm - B_{1,\xi}^\pm\phi_{i,\xi}^\pm, \quad \text{at } \eta = \mp\frac{\delta}{2} + B_1^\pm(\xi), \quad (102)$$

$$3\phi_i^+ - 2\xi\phi_{i,\xi}^+ - 2\eta\phi_{i,\eta}^+ - \gamma\left[3\phi_i^- - 2\xi\phi_{i,\xi}^- - 2\eta\phi_{i,\eta}^-\right] + (1-\gamma)\eta, \quad (103)$$
$$= \frac{1}{2}\left[\gamma|\nabla\phi_i^-|^2 - |\nabla\phi_i^+|^2\right], \quad \text{at } \xi = H_1(\eta),$$

$$2H_1 - 2\eta H_{1,\eta} = \phi_{i,\xi}^+ - H_{1,\eta}\phi_{i,\eta}^+, \quad \text{at } \xi = H_1(\eta), \quad (104)$$

$$\phi_i^+ \to -\delta\eta + \frac{1}{6}\left(\frac{2+\gamma}{1+\gamma}\delta^2 + \frac{\Gamma}{2\pi}\theta + b^+\right) + o(1), \quad \text{as } \rho \to \infty, \quad (105)$$

$$\phi_i^- \to \delta\eta + \frac{1}{6}\left(\frac{1+2\gamma}{1+\gamma}\delta^2 + \frac{\Gamma}{2\pi}\theta + b^-\right) + o(1), \quad \text{as } \rho \to \infty, \quad (106)$$

$$H_1(\eta) \to -\frac{\Gamma}{48\pi}\frac{1}{\eta} + o\left(\frac{1}{\eta}\right), \quad \text{as } \rho \to \infty, \quad (107)$$

$$B_1^\pm(\xi) \to \frac{\Gamma}{48\pi}\frac{1}{\xi} + o\left(\frac{1}{\xi}\right), \quad \text{as } \rho \to \infty, \quad (108)$$

where $\rho = \sqrt{\xi^2 + \eta^2}$.

Equations (101) and (102) are the dynamic and kinematic free surface conditions at the horizontal free surfaces, and (103) and (104) are the conditions at the interface. The functions $\phi_i^\pm(\xi, \eta, t)$ are harmonic functions of ξ and η. The unknown functions appearing in (101)–(104), $\phi_i^\pm(\xi, \eta, t)$, $B_1^\pm(\xi, t)$, and $H_1(\eta, t)$, have to be matched with the outer solution given by (105)–(108) in the far field as $\rho \to \infty$. The boundary value problem (101)–(108) for the inner velocity potentials and the shapes of the free surfaces and the interface is too complicated to be solved by analytical means. A numerical method such as boundary element method should be employed to solve this problem, which will not be pursued in this paper.

However, we can find the behavior of the inner solution at the far field by defining new potentials $\Phi_i^\pm$, and new free surfaces ($b_1^\pm$) and interface (h_1) shapes

$$\phi_i^+ + \delta\eta - \frac{1}{6}\left(\frac{2+\gamma}{1+\gamma}\delta^2 + \frac{\Gamma}{2\pi}\theta + b^+\right) = \Phi_i^+,$$
$$\phi_i^- - \delta\eta - \frac{1}{6}\left(\frac{1+2\gamma}{1+\gamma}\delta^2 + \frac{\Gamma}{2\pi}\theta + b^-\right) = \Phi_i^-$$
$$B_1^\pm(\xi) - \frac{\Gamma}{48\pi\xi} = b_1^\pm(\xi), \quad (109)$$
$$H_1(\eta) - \frac{\Gamma}{48\pi\eta} = h_1(\eta).$$

After substituting the Eq. (109) in the conditions (101)–(108), we obtain the new boundary conditions

$$3\Phi_i^+ - 2\xi\Phi_{i,\xi}^+ - 2\eta\Phi_{i,\eta}^+$$
$$= -\frac{1}{2}|\nabla\Phi_i^+|^2 + \frac{\Gamma}{12\pi}\frac{1}{\rho^2}\left(\eta\Phi_{i,\xi}^+ - \xi\Phi_{i,\eta}^+\right) + \delta\Phi_{i,\eta}^+$$
$$- \frac{1}{2}\left(\frac{1}{6}\frac{\Gamma}{2\pi}\right)^2\frac{1}{\rho^2} + \frac{\Gamma}{12\pi}\frac{\xi\delta}{\rho^2} - \eta(1-\delta) - \frac{\Gamma}{4\pi}\theta$$
$$+ \frac{\gamma(\gamma-1)(\gamma-7)}{(1+\gamma)^3}, \text{ at } \eta = -\frac{\delta}{2} + \frac{\Gamma}{48\pi\xi} + b_1^+(\xi), \quad (110)$$

$$3\Phi_i^- - 2\xi\Phi_{i,\xi}^- - 2\eta\Phi_{i,\eta}^-$$
$$= -\frac{1}{2}|\nabla\Phi_i^-|^2 + \frac{\Gamma}{12\pi}\frac{1}{\rho^2}\left(\eta\Phi_{i,\xi}^- - \xi\Phi_{i,\eta}^-\right) - \delta\Phi_{i,\eta}^- - \frac{1}{2}\left(\frac{1}{6}\frac{\Gamma}{2\pi}\right)^2\frac{1}{\rho^2}$$
$$- \frac{\Gamma}{12\pi}\frac{\xi\delta}{\rho^2} - \eta(1+\delta) - \frac{\Gamma}{4\pi}\theta + \frac{(1-\gamma)(5\gamma+1)}{(1+\gamma)^3},$$
$$\text{at } \eta = \frac{\delta}{2} + \frac{\Gamma}{48\pi\xi} + b_1^-(\xi), \quad (111)$$

$$2\eta - 2\xi B_{1,\xi}^{+} = \Phi_{i,\eta}^{+} - \delta + \frac{\Gamma}{12\pi}\frac{\xi}{\rho^2} - B_{1,\xi}^{+}\left(\Phi_{i,\xi}^{+} - \frac{\Gamma}{12\pi}\frac{\eta}{\rho^2}\right),$$

$$\text{at } \eta = -\frac{\delta}{2} + \frac{\Gamma}{48\pi\xi} + b_1^{+}(\xi), \qquad (112)$$

$$2\eta - 2\xi B_{1,\xi}^{-} = \Phi_{i,\eta}^{-} + \delta + \frac{\Gamma}{12\pi}\frac{\xi}{\rho^2} - B_{1,\xi}^{-}\left(\Phi_{i,\xi}^{-} - \frac{\Gamma}{12\pi}\frac{\eta}{\rho^2}\right),$$

$$\text{at } \eta = \frac{\delta}{2} + \frac{\Gamma}{48\pi\xi} + b_1^{-}(\xi), \qquad (113)$$

$$3\Phi_i^{+} - 2\xi\Phi_{i,\xi}^{+} - 2\eta\Phi_{i,\eta}^{+} - 3\gamma\Phi_i^{-} + 2\gamma\xi\Phi_{i,\xi}^{-} + 2\gamma\eta\Phi_{i,\eta}^{-} + \frac{\Gamma\theta}{4\pi}(1-\gamma)$$

$$-6\gamma\frac{(1-\gamma)^2}{(1+\gamma)^3} = \frac{\gamma}{2}|\nabla\Phi_i^{-}|^2 - \frac{1}{2}|\nabla\Phi_i^{+}|^2 + \frac{\gamma-1}{2}\left(\frac{\Gamma}{12\pi}\right)^2\frac{1}{\rho^2}$$

$$+(1+\gamma)\frac{\Gamma}{12\pi}\frac{\xi\delta}{\rho^2} + \frac{\Gamma}{12\pi}\frac{\eta}{\rho^2}\left(-\gamma\Phi_{i,\xi}^{-} + \Phi_{i,\xi}^{+}\right) + \frac{\Gamma}{12\pi}\frac{\xi}{\rho^2}\left(\gamma\Phi_{i,\eta}^{-} - \Phi_{i,\eta}^{+}\right)$$

$$+\delta\left(\gamma\Phi_{i,\eta}^{-} + \Phi_{i,\eta}^{+}\right), \quad \text{at } \xi = -\frac{\Gamma}{48\pi\eta} + h_1(\eta), \qquad (114)$$

$$2H_1 - 2\eta H_{1,\eta} = \Phi_{i,\xi}^{+} - \frac{\Gamma}{12\pi}\frac{\eta}{\rho^2} - H_{1,\eta}\left(\Phi_{i,\eta}^{+} - \delta + \frac{\Gamma}{12\pi}\frac{\xi}{\rho^2}\right),$$

$$\text{at } \xi = -\frac{\Gamma}{48\pi\eta} + h_1(\eta), \qquad (115)$$

$$\text{As } \rho \to \infty, \quad \Phi_i^{\pm} = o(1), b_1^{\pm} = o(1/\xi), H_1 = o(1/\eta). \qquad (116)$$

In the far field, the conditions (110)–(115) become

$$3\Phi_i^{+} - 2\xi\Phi_{i,\xi}^{+} = \frac{\Gamma(5\delta-1)}{48\pi\xi}, \quad \text{as } \xi \to \infty \text{ and } \eta \to -\delta/2, \qquad (117)$$

$$3\Phi_i^{-} - 2\xi\Phi_{i,\xi}^{-} = -\frac{\Gamma(5\delta+1)}{48\pi\xi}, \quad \text{as } \xi \to -\infty \text{ and } \eta \to \delta/2, \qquad (118)$$

$$2b_1^{+} - 2\xi b_{1,\xi}^{+} = \Phi_{i,\eta}^{+}, \quad \text{as } \xi \to \infty \text{ and } \eta \to -\delta/2, \qquad (119)$$

$$2b_1^{-} - 2\xi b_{1,\xi}^{-} = \Phi_{i,\eta}^{-}, \quad \text{as } \xi \to -\infty \text{ and } \eta \to \delta/2, \qquad (120)$$

$$3(\Phi_i^{+} - \gamma\Phi_i^{-}) = 2\eta(\Phi_{i,\eta}^{+} - \gamma\Phi_{i,\eta}^{-}), \quad \text{as } \xi \to 0 \text{ and } \eta \to -\infty, \qquad (121)$$

$$2h_1 - 2\eta h_{1,\eta} = \frac{\delta\Gamma}{48\pi\eta^2}, \quad \text{as } \xi \to 0 \text{ and } \eta \to -\infty. \qquad (122)$$

The functions $b_1^{\pm}(\xi)$ in (119) and (120) behave as $1/\xi^3$ and $h_1(\eta)$ in (122) behaves as $1/\eta^2$ in the far-field, where $\rho \to \infty$. The potentials $\Phi_i^{\pm}$ and the functions $b_1^{\pm}, h_1$ can be determined from the boundary value problem (117)–(122) as

$$\Phi_i^{+} = A_i^{+}\frac{\cos\theta}{\rho} + C\gamma\frac{\sin\theta}{\rho},$$

$$\Phi_i^{-} = A_i^{-}\frac{\cos(\theta-\pi)}{\rho} + C\frac{\sin(\pi-\theta)}{\rho}, \qquad (123)$$

$$b_1^{+} = \pm\frac{\delta A_i^{\pm}}{16}\frac{1}{\xi^3}, \quad h_1 = \frac{1}{6}\frac{\Gamma}{48\pi}\frac{1}{\eta^2},$$

where

$$A_i^{+} = \frac{\Gamma}{48\pi}\frac{5\delta-1}{5}, \quad A_i^{-} = -\frac{\Gamma}{48\pi}\frac{5\delta+1}{5},$$

and C is an arbitrary constant. The second terms in $\Phi_i^{\pm}$ (123) are the eigen solutions of the boundary value problem (117), (118), and (121). Hence, the behavior of the inner solution in the far field is given by

$$\phi_i^{+} \sim -\delta\eta + \frac{1}{6}\left(\frac{2+\gamma}{1+\gamma}\delta^2 + \frac{\Gamma}{2\pi}\theta + b^{+}\right) + A_i^{+}\frac{\cos\theta}{\rho} + C\gamma\frac{\sin\theta}{\rho} + o(\rho^{-1}),$$
$$(124)$$

$$\phi_i^{-} \sim \delta\eta + \frac{1}{6}\left(\frac{1+2\gamma}{1+\gamma}\delta^2 + \frac{\Gamma}{2\pi}\theta + b^{-}\right) + A_i^{-}\frac{\cos(\theta-\pi)}{\rho}$$
$$+ C\frac{\sin(\pi-\theta)}{\rho} + o(\rho^{-1}).$$

The unknown constant C in (124) could be determined numerically (Ref. 20 for details), which will not be pursued in this paper. The refined far-field behaviors of the inner potentials (124) are useful for the numerical solution of the inner region flow problem (101)–(108). The shapes of the interface and the free surfaces in the far-field predicted by (124) using Lagrangian variables are shown in Fig. 9. We may conclude that the flow in the far field of the inner region is dominated by the vortex with strength Γ.

VII. CONCLUSIONS

Short-time behavior of gravity-driven free surface flow of two fluids of equal depth was studied. Attention was paid to the motions of the interface and the free surfaces as well as the singular behaviors of the velocity field at the bottom point, where the interface meets the rigid bottom, and the top point, where the interface meets the free surfaces. The leading-order linear problem is solved by the Fourier series method. The shapes of the free surfaces and the interface in the leading order computed by using the Lagrangian variables show a jump discontinuity of the free surface near the top point where the free surfaces and the interface meet. The second-order solution does not resolve the discontinuity problem of the free surfaces at the top point, but is required to formulate inner problems near the points of singularity.

Inner region formulation was derived for the top point. The far-field behavior of the inner flow was obtained, which will be helpful for the numerical solution of the inner region problem.

The flow velocity provided by the outer solution was shown to be log-singular at the bottom point. The leading-order inner asymptotic
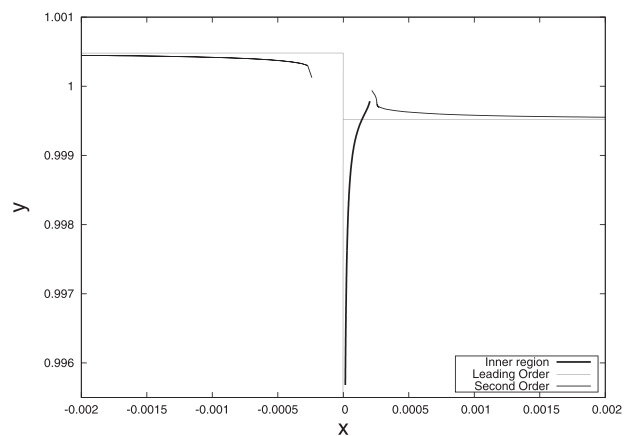

FIG. 9. The shape of the interface and the free surfaces in nondimensional variables close to the point (0, 1), for $t = 1.2$, $\epsilon = 0.002$, and $\gamma = 0.5$.

solution was found near this point. The inner flow close to the bottom point is self-similar. It was shown that the shape of the interface is independent of any parameters in specially stretched inner variables. In the limiting case when the fluid on the left disappears ($\gamma = 0$), we recover the results of Ref. 16 exactly. The important parameter in the present analysis is $\delta = (1-\gamma)/(1+\gamma)$, which appears as a product in the first-order potentials and the free surfaces. The parameter δ appears again in the leading-order asymptotic solution.

We see that as $\gamma = \rho^-/\rho^+$, $0 \leq \gamma \leq 1$ increases, the shape of the interface at the bottom becomes more rounded. This means that the angle between the interface and the bed increases with increase in δ; that is, the jet is less pronounced as the density ratio becomes smaller.

The inner region calculations carried out near the bottom point in this paper is valid for any two-dimensional dam break problem involving two fluids with different heights. This is because locally, close to the bottom point, heights of the fluids do not matter. Therefore, the obtained leading-order solution is valid for any heights of the fluids.

The neglect of the viscous effects from the present analysis is justified by comparing the order of magnitude of the acceleration and the viscous terms in the momentum equation. In the main flow region, the order of the acceleration term is $O(gt)$ and the order of the viscous term is $O(\nu t \sqrt{\epsilon g}/H^{3/2})$. The ratio of the two terms for fresh water is $\frac{|\nu \nabla^2 \mathbf{u}|}{\mathbf{u_t}} = 3.2 \times 10^{-7} \frac{\sqrt{\epsilon}}{H^{3/2}}$, where for kinematic viscosity, $\nu = 1.0034 \times 10^{-6}$ m²/s (Ref. 21) is used. The ratio of the viscous and acceleration terms is quite small, and it is safe to ignore the viscous effects in the main flow region. However, close to the top and bottom points the effect of viscosity could be larger than that in the main flow region. Near the bottom point (0, 0), the order of the acceleration term is $O(g/a)$ and the order of the viscous term is $O(\nu \sqrt{\epsilon g}/(H^{3/2}a^3))$ and the ratio of the two terms for fresh water is $\frac{|\nu \nabla^2 \mathbf{u}|}{\mathbf{u_t}} = 3.2 \times 10^{-7} \frac{\sqrt{\epsilon}}{H^{3/2}a^2}$. The viscous effects for the bottom point are considerably larger than those in the main flow region. This is especially true when the size of the inner region, a, is too small that is for very short times. For example, when $\epsilon \approx a = 7 \times 10^{-5}$, then the viscosity is as important as the inertia. Hence, unless we are dealing with very short times [that is when $\epsilon = O(10^{-5})$ or smaller], the viscosity is negligible near the bottom point. Exactly, the same conclusion is drawn for the top point (0, 1). The magnitude of order calculations for the top point is similar to those for the bottom point.

ACKNOWLEDGMENTS

AUTHOR DECLARATIONS
Conflict of Interest

The authors have no conflicts to disclose.

Author Contributions

Alexander Korobkin: Conceptualization (equal); Formal analysis (equal); Investigation (equal); Methodology (equal); Visualization (equal); Writing – original draft (equal); Writing – review & editing (equal). **Oguz Yilmaz:** Formal analysis (equal); Investigation (equal); Methodology (equal); Software (equal); Visualization (equal); Writing – original draft (equal); Writing – review & editing (equal).

DATA AVAILABILITY

The data that support the findings of this study are available within the article.

APPENDIX A: REGULAR COMPONENTS OF THE SECOND-ORDER VELOCITY POTENTIALS

The decomposition (30) of the potentials $\phi^\pm$, which satisfy Laplace's equations in the corresponding domains, into regular and singular parts provides the following boundary conditions for the regular potentials $\phi_R^\pm(x,y)$ using the boundary conditions (23)–(25) for the free surfaces and interface

$$\phi_R^+ - \gamma\phi_R^- = A_R \frac{1}{(y-2)^2} + B_R \frac{1}{(y+2)^2} + 3\frac{(\gamma-1)^3}{(\gamma+1)^2} \quad (x=0, 0<y<1), \tag{A1}$$

$$\phi_{R,x}^+ = \phi_{R,x}^- \quad (x=0, 0<y<1), \tag{A2}$$

$$\phi_R^+ = \frac{4\delta}{\pi}\arctan(e^{-\pi x/2}) - \frac{4+3\gamma}{1+\gamma}\frac{16\delta^2}{\pi^2}\arctan^2(e^{-\pi x/2}), \tag{A3}$$

$$-(\Gamma+B^+)\frac{1-x^2}{(1+x^2)^2} - \left(-\frac{\Gamma}{2\pi}\arctan\frac{2}{x}+B^+\right)\frac{9-x^2}{(9+x^2)^2}$$
$$+\frac{\Gamma}{2\pi}\frac{3x}{(9+x^2)^2}\log(x^2+4) + \frac{\Gamma}{2\pi}\frac{2x}{(1+x^2)^2}\log|x| \quad (y=1, x>0),$$

$$\phi_R^- = -\frac{4\delta}{\pi}\arctan(e^{\pi x/2}) - \frac{3+4\gamma}{1+\gamma}\frac{16\delta^2}{\pi^2}\arctan^2(e^{\pi x/2}) \tag{A4}$$

$$-(\Gamma/2+B^-)\frac{1-x^2}{(1+x^2)^2} - \left(-\frac{\Gamma}{2\pi}\arctan\frac{2}{x}+B^-\right)\frac{9-x^2}{(9+x^2)^2}$$
$$+\frac{\Gamma}{2\pi}\frac{3x}{(9+x^2)^2}\log(x^2+4) + \frac{\Gamma}{2\pi}\frac{2x}{(1+x^2)^2}\log|x| \quad (y=1, x<0),$$

$$\phi_{R,y}^\pm = 0 \quad (y=0), \tag{A5}$$

where

$$A_R = \frac{\Gamma}{40}(5+13\gamma) + \frac{9}{10}\gamma\phi^-(0,1) - \frac{9}{10}\phi^+(0,1),$$

$$B_R = \frac{9\Gamma}{40}(5-3\gamma) + \frac{9}{10}\gamma\phi^-(0,1) - \frac{9}{10}\phi^+(0,1),$$

and the range of the arctangent function is between $-\pi/2$ and $\pi/2$. At the triple point, $x=0$ and $y=1$, $\phi_R^\pm = 0$ and the boundary conditions are consistent there. In addition to the condition (A1)–(A5), the functions $\phi_R^\pm$ should also satisfy the conditions at infinity

$$\phi_R^+ \to 0 (x \to +\infty), \quad \phi_R^- \to 0 (x \to -\infty). \tag{A6}$$

The function $\phi_R^\pm$ is further decomposed as

$$\phi_R^\pm = \phi_{R0} + \phi_{R1}^\pm, \tag{A7}$$

where the potential ϕ_{R0} is continuous across the interface and satisfies the free surface conditions, (A3) and (A4),

$$\phi_{R0} = \frac{4\delta}{\pi}\arctan(e^{-\pi x/2}) - \frac{4+3\gamma}{1+\gamma}\frac{16\delta^2}{\pi^2}\arctan^2(e^{-\pi x/2})$$
$$-(\Gamma+B^+)\frac{1-x^2}{(1+x^2)^2} - \left(-\frac{\Gamma}{2\pi}\arctan\frac{2}{x}+B^+\right)\frac{9-x^2}{(9+x^2)^2}$$
$$+\frac{\Gamma}{2\pi}\frac{3x}{(9+x^2)^2}\log(x^2+4)+\frac{\Gamma}{2\pi}\frac{2x}{(1+x^2)^2}\log|x| \ (y=1,x>0),$$

(A8)

$$\phi_{R0} = -\frac{4\delta}{\pi}\arctan(e^{\pi x/2}) - \frac{3+4\gamma}{1+\gamma}\frac{16\delta^2}{\pi^2}\arctan^2(e^{\pi x/2})$$
$$-(\Gamma/2+B^-)\frac{1-x^2}{(1+x^2)^2} - \left(-\frac{\Gamma}{2\pi}\arctan\frac{2}{x}+B^-\right)\frac{9-x^2}{(9+x^2)^2}+$$
$$+\frac{\Gamma}{2\pi}\frac{3x}{(9+x^2)^2}\log(x^2+4)+\frac{\Gamma}{2\pi}\frac{2x}{(1+x^2)^2}\log|x| \ (y=1,x<0),$$

the boundary condition (A5) at $y=0$ and the conditions at infinity (A6). The potentials $\phi_{R1}^\pm$ are zero at the free surface and satisfy the conditions (A1) and (A2) at the interface

$$\phi_{R1}^+ - \gamma\phi_{R1}^- = A_R\frac{1}{(y-2)^2} + B_R\frac{1}{(y+2)^2} +$$
$$3\frac{(\gamma-1)^3}{(\gamma+1)^2} + \phi_{R0}(\gamma-1), \ x=0, 0<y<1,$$

(A9)

$$\phi_{R1,x}^+ = \phi_{R1,x}^-, \quad x=0, 0<y<1,$$

(A10)

the boundary condition (A5) at $y=0$ and the conditions at infinity (A6).

The harmonic function ϕ_{R0} in the strip $0<y<1, -\infty<x<\infty$ is obtained by the Fourier transform in x,

$$\phi_{R0}(x,y) = \int_{-\infty}^{\infty} \phi_{R0}(s,1)\frac{\cos\frac{\pi y}{2}\cosh\frac{\pi(s-x)}{2}}{\cosh(\pi(s-x))+\cos(\pi y)}ds, \quad (A11)$$

where $\phi_{R0}(s,1)$ is given by (A8).

The potentials $\phi_{R1}^\pm(x,y)$ are sought in the form (11)

$$\phi_{R1}^+(x,y) = \sum_{n=0}^{\infty} C_n e^{-\mu_n x}\cos(\mu_n y),$$

(A12)

$$\phi_{R1}^-(x,y) = \sum_{n=0}^{\infty} D_n e^{\mu_n x}\cos(\mu_n y),$$

(A13)

where C_n and D_n are unknown coefficients to be determined from the interface conditions (A9) and (A10). The kinematic interface condition (A10) gives that $-C_n = D_n$, and from the dynamic condition (A9), we obtain

$$(1+\gamma)\frac{C_n}{2} = A_R I_{1n} + B_R I_{2n} + C_R\frac{(-1)^n}{\mu_n}$$
$$+(\gamma-1)\int_0^1 \phi_{R0}(0,y)\cos(\mu_n y)dy,$$

where

$$I_{1n} = \int_0^1 \frac{\cos(\mu_n y)}{(y-2)^2}dy, \quad I_{2n} = \int_0^1 \frac{\cos(\mu_n y)}{(y+2)^2}dy, \quad C_R = 3\frac{(\gamma-1)^3}{(\gamma+1)^2}. \quad (A14)$$

The integrals I_{1n} and I_{2n} for large n behave as

$$I_{1n} = \frac{(-1)^n}{\mu_n} - \frac{1}{4\mu_n^2} + O(1/\mu_n^3),$$
$$I_{2n} = \frac{(-1)^n}{9\mu_n} + \frac{1}{4\mu_n^2} + O(1/\mu_n^3).$$

(A15)

The asymptotic formulas (A15) are used in numerical evaluations of the integrals in (A14).

APPENDIX B: THE SHAPES OF THE FREE SURFACES AND THE INTERFACE IN THE MAIN FLOW REGION

The free surface and interface shapes are given by

$$y = 1 + \epsilon Y^\pm(x,t), \quad x = \epsilon X(y,t),$$

where $Y^\pm(x,t)$ and $X(y,t)$ are given by (9)

$$Y^\pm(x,t,\epsilon) = \frac{1}{2}t^2\varphi_{0,y}^\pm(x,1) + \frac{1}{24}\epsilon t^4 Y_1^\pm(x) + \cdots,$$
$$X(y,t,\epsilon) = \frac{1}{2}t^2\varphi_{0,x}^\pm(0,y) + \frac{1}{24}\epsilon t^4 X_1(y) + \cdots.$$

(B1)

The leading-order terms in (B1) are calculated using the results of Sec. III,

$$\varphi_{0,y}^\pm(x,1) = \mp\frac{4\delta}{\pi}\arctan\left(\exp\left(\mp\frac{\pi x}{2}\right)\right),$$
$$\varphi_{0,x}^\pm(0,y) = \frac{2\delta}{\pi}\log\left(\tan\left(\frac{\pi y}{4}\right)\right).$$

(B2)

For the second-order terms in (B1), Eqs. (18), (20)–(22), and (30)–(32) are used

$$Y_1^\pm(x) = \varphi_{1,y}^\pm(x,1) = \phi_y^\pm(x,1),$$

(B3)

$$\phi_y^\pm(x,1) = \phi_{S,y}^\pm(x,1) + \phi_{R0,y}(x,1) + \phi_{R1,y}^\pm(x,1),$$

(B4)

$$X_1(y) = \varphi_{1,x}^\pm(0,y)\pm\frac{3\delta^2}{\sin(\pi y/2)},$$

(B5)

$$\varphi_{1,x}^+ = -2\frac{2+\gamma}{1+\gamma}\frac{\delta^2}{\sin(\pi y/2)} + \phi_x^+(0,y),$$

(B6)

$$\varphi_{1,x}^- = 2\frac{1+2\gamma}{1+\gamma}\frac{\delta^2}{\sin(\pi y/2)} + \phi_x^-(0,y),$$

(B7)

$$\phi_x^\pm(0,y) = \phi_{S,x}^\pm(0,y) + \phi_{R0,x}(0,y) + \phi_{R1,x}^\pm(0,y).$$

(B8)

The derivatives $\phi_{S,y}^\pm(x,1)$ in (B4) and $\phi_{S,x}^\pm(0,y)$ in (B8) are calculated using (31). To calculate the terms $\phi_{R0,y}(x,1)$ and $\phi_{R0,x}(0,y)$, (A11) is used. The potentials $\phi_{R1}^\pm(x,y)$ are given by the series (A12) and (A13), and their derivatives can be readily calculated.

REFERENCES

[1] J. E. Simpson, D. A. Mansfield, and J. R. Milford, "Inland penetration of sea-breeze fronts," Q. J. R. Meteorol. Soc. **103**, 47–76 (1977).

[2] J. R. L. Allen, "Mixing at turbidity current heads, and its geological implications," J. Sediment. Petrol. **41**, 97–113 (1971).

[3] D. P. Hoult, "Oil spreading on the sea," Annu. Rev. Fluid Mech. **4**, 341–368 (1972).

20 February 2024 12:34:50

[4]J. E. Simpson, "Gravity currents in the laboratory, atmosphere and ocean," Annu. Rev. Fluid Mech. **14**, 213–234 (1982).

[5]J. W. Rottman and J. E. Simpson, "Gravity currents produced by instantaneous releases of a heavy fluid in a rectangular channel," J. Fluid Mech. **135**, 95–110 (1983).

[6]S. J. D. D'Alessio, T. Bryant Moodie, J. P. Pascal, and G. E. Swaters, "Gravity currents produced by sudden release of a fixed volume of a heavy fluid," Stud. Appl. Math. **96**, 359–385 (1996).

[7]S. K. Ooi, G. Constantinescu, and L. Weber, "Numerical simulations of lock exchange compositional gravity current," J. Fluid Mech. **635**, 361–388 (2009).

[8]J. G. Esler and J. D. Pearce, "Dispersive dam break and lock exchange flows in a two layer fluid," J. Fluid Mech. **667**, 555–585 (2011).

[9]P. E. Tyvand and T. Miloh, "Free-surface flow due to impulsive motion of a submerged circular cylinder," J. Fluid Mech. **286**, 67–101 (1995).

[10]C. Adduce, G. Sciortine, and S. Proietti, "Gravity currents produced by lock exchanges: Experiments and simulations with a two layer shallow water model with entrainment," J. Hydraul. Eng. **138**, 111–121 (2012).

[11]T. I. Khabakhpasheva and A. A. Korobkin, "Blunt body impact onto viscoelastic floating ice plate with a soft layer on its upper surface," Phys. Fluids **33**(6), 062105 (2021).

[12]Y. Z. Xue, L. D. Zeng, B. Y. Ni, A. A. Korobkin, and T. I. Khabakhpasheva, "Hydroelastic response of an ice sheet with a lead to a moving load," Phys. Fluids **33**(3), 037109 (2021).

[13]T. I. Khabakhpasheva and A. A. Korobkin, "Splashing of liquid droplet on a vibrating substrate," Phys. Fluids **32**(12), 122109 (2020).

[14]T. I. Khabakhpasheva and A. A. Korobkin, "Oblique elastic plate impact on thin liquid layer," Phys. Fluids **32**(6), 062101 (2020).

[15]A. A. Korobkin, T. I. Khabakhpasheva, and S. Malenica, "Maximum stress of stiff elastic plate in uniform flow and due to jet impact," Phys. Fluids **29**(7), 072105 (2017).

[16]A. Korobkin and O. Yilmaz, "The initial stage of dam break flow," J. Eng. Math. **63**, 293–308 (2009).

[17]O. Yilmaz, A. Korobkin, and A. Iafrati, "The initial stage of dam break flow of two immiscible fluids. Linear analysis of global flow," Appl. Ocean Res. **42**, 60–69 (2013).

[18]K. A. Shishmarev, T. I. Khabakhpasheva, and A. A. Korobkin, "Theoretical analysis of time-dependent jetting on the surface of a thin moving liquid layer," Phys. Fluids **34**(3), 032103 (2022).

[19]A. C. King and D. J. Needham, "The initial development of a jet caused by fluid, body and free surface interaction. Part 1. A uniformly accelerating plate," J. Fluid Mech. **268**, 89–101 (1994).

[20]A. Iafrati and A. Korobkin, "Initial stage of flat plate impact onto liquid free surface," Phys. Fluids **16**, 2214–2227 (2004).

[21]IITC, *ITTC Recommended Procedures. Fresh Water and Sea Water Properties* (IITC, 2011).